

# Final Technical Report

## Project Title:

*Geodetic Constraints on Fault Slip Rates and Seismic Hazard in the Greater Las Vegas Area*

**Award number:** *G13AP0018*

## Principal Investigator:

*Cornelis Kreemer, [cornelisk@unr.edu](mailto:cornelisk@unr.edu)*

## Co-Investigator:

*William C. Hammond, [whammond@unr.edu](mailto:whammond@unr.edu)*

## Contact Information:

*Nevada Bureau of Mines and Geology  
University of Nevada, Reno  
1664 N. Virginia Street, Reno, NV 89557  
Tel: 775-682-8780; Fax: 775-784-1709*

## Start and End Dates of this 12 Month Project:

*April 1, 2013 to March 31, 2014*

## Abstract

Active crustal deformation associated with the motion of the Pacific Plate relative to stable North America loads faults in southern Nevada, posing a seismic hazard to the city of Las Vegas and surrounding smaller communities. We reoccupied a part of the existing MAGNET GPS network of geodetic markers in the greater Las Vegas area to fill in gaps in the coverage and improve constraints on velocities of existing stations. Our measurements found rates of motion on many markers for the first time, placing new and stronger constraints on the localization of strain accumulation and fault slip rates. We measured 24 stations which now have a minimum of 7 years between their first and last observation. From these measurements we estimated the velocity of crustal motion for each station. We account for deformation from the 2010 El Mayor-Cucapah earthquake in northern Baja California that caused detectable co- and post seismic deformation in the network. From this new velocity field we generated a horizontal tensor strain rate map and a crustal block motion model to estimate slip rates on active faults in area. The measurements reveal active deformation distributed across southern Nevada, eastern California and western Arizona. We find that  $\sim 2$  mm/yr of extensional strain is distributed over about  $\sim 200$  km centered on Las Vegas, giving a strain accumulation rate that intermediate between that of the Walker Lane and eastern Nevada. Faults in the Las Vegas Valley, including the Eglington and Frenchman Mountain faults, slip at rates typical of the region, having normal slip rates (projected into the horizontal plate) near 0.2 mm/yr.

## Report

### Background

Seismic source information that feeds into the current National Seismic Hazard Maps (NSHM) principally comes from seismic recordings of earthquakes and paleoseismic constraints on past earthquake occurrence. The relative quiescence in most of southern Nevada and the absence of many recognized Quaternary faults capable of causing an  $M > 7$  event implies that the current NSHM (*Petersen et al.*, 2008) has assigned a relatively low probability of exceeding Peak Ground Acceleration (PGA) levels in and around Las Vegas, Nevada. However, previous geologic studies of deformation have identified structures that indicate substantial shear and extension have occurred (e.g. see *Faulds and Henry*, 2008 for summary). Furthermore, the rate of present-day extension across  $\sim 100$  km surrounding the greater Las Vegas area is much larger than what is documented in the few Quaternary faults in the area. Data from long-running GPS sites in the region now unequivocally show that  $\sim 2$  mm/yr extension takes place between the Eastern California Shear Zone (ECSZ) and the Colorado Plateau (CP) at the latitude of Las Vegas (*Kreemer et al.*, 2010). The rates of extension are greater than in northeast Nevada, where the 2008 Wells, NV  $M 6.0$  earthquake occurred.

The goal of this project is to identify the nature and localization of the deformation in the region surrounding Las Vegas, Nevada, using GPS measurements of markers established in 2007, with the specific goal to establish which of the regional fault structures/zones are likely active and at what rate. In order to assess the threat this seismic hazard poses to the Las Vegas area, it is necessary to constrain where the  $\sim 2.1$  mm/yr extension is distributed and whether it could be localized across Las Vegas metropolitan area faults. To answer these important questions we have filled in gaps in the previously existing GPS coverage, and refined the crustal velocity field by re-measuring a dense array of stable geodetic markers in the semi-permanent MAGNET GPS network.

### Data Collection, Processing, and Analysis

In 2013 and 2014 we occupied MAGNET GPS sites and collected data for 3 to 4 weeks each time. Many of these stations had been installed in 2007 and measured for  $\sim 4$  weeks so the resulting time series are now up to 7 years in duration (interval of time between first and last observation). We combined these data together with data from other high-quality continuous GPS sites in the region (from e.g. the NSF EarthScope Plate Boundary Observatory and CORS network) to obtain a dense velocity field and model the regional surface motions in terms of the strain accumulation (which drives future seismic moment release), micro-block motions, and slip rates on the block-bounding faults. These data collected during this project have been archived at UNAVCO and are available to anyone online via Geodetic Seamless Archive Center (<http://www.unavco.org/software/data-management/gnac/gnac.html>).

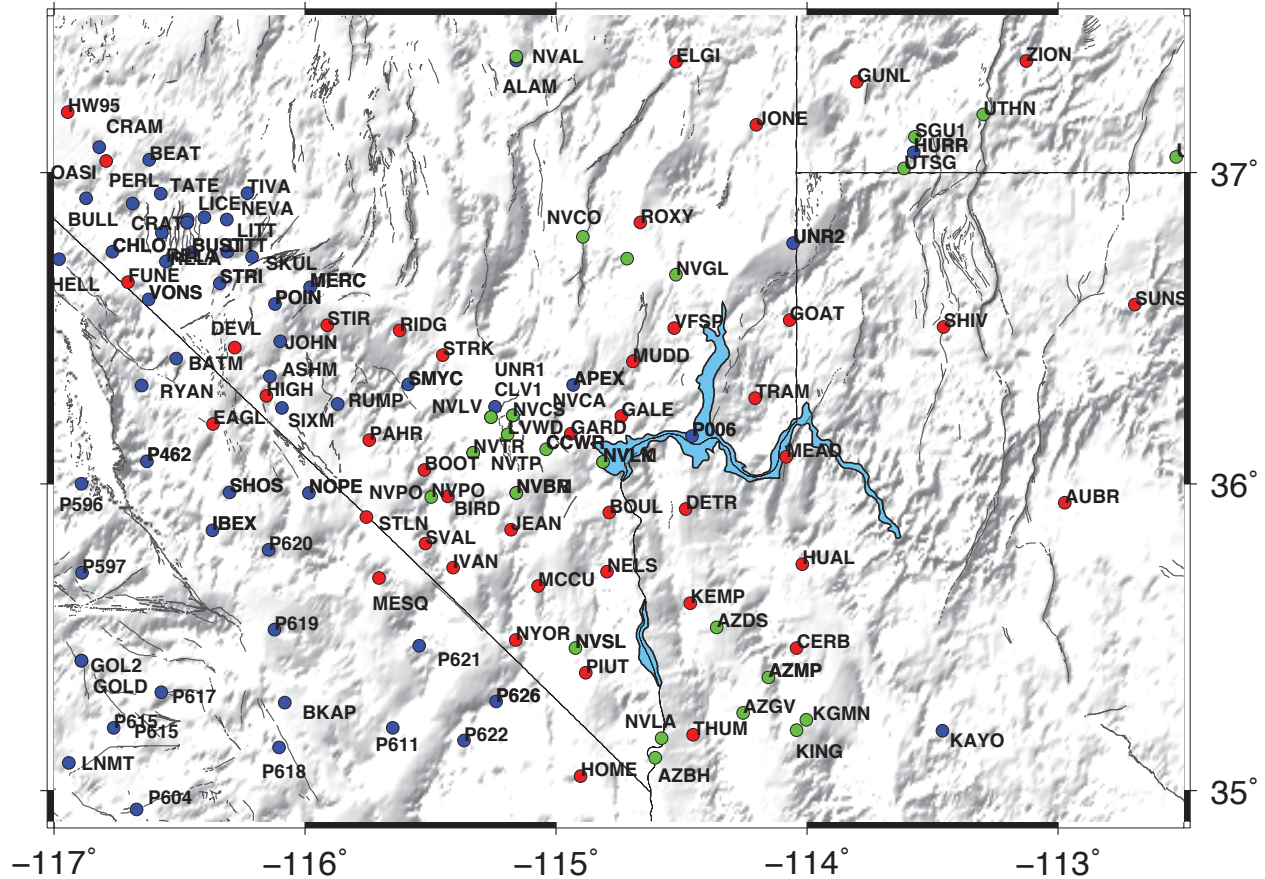


**Figure 1.** Sites surveyed and from which data were used for this study. MAGNET GPS network semi-continuous stations (red) were surveyed in 2013 and 2014. We also used data from other continuous stations (blue) and from CORS stations (green). Station 4-character IDs are given at each station.

### GPS Data Processing

The data were processed as a part of a >12,000 station mega-network analysis system that retrieves data daily and updates solutions weekly. We use the GIPSY/OASIS software provided by the Jet Propulsion Laboratory (JPL) to estimate station coordinates every 24 hours using the Precise Point Positioning (PPP) method (Zumberge *et al.*, 1997). Ionosphere-free combinations of carrier phase and pseudorange were obtained every 5 minutes. Calibrations were applied for all antennas, ground receivers, and satellite transmitters. To model tropospheric refractivity, the Global Mapping Function was applied (Boehm *et al.*, 2006), with tropospheric wet zenith delay and horizontal gradients estimated as stochastic random-walk parameters every 5 minutes (Bar-Sever *et al.*, 1998). The observable model includes ocean tidal loading (including companion tides) coefficients supplied by Chalmers University (Scherneck *et al.*, 1991). Ambiguity resolution was applied to double differences of the estimated one-way bias parameters (Blewitt, 1989), using the wide lane and phase bias method, which phase-connects individual stations to IGS stations in common view (Bertiger *et al.*, 2010). Satellite orbit and clock parameters were

provided by JPL, who determine these parameters in a global fiducial-free analysis using a subset of the available IGS core stations as tracking sites. A more detailed description of the data processing strategy and parameters used in the processing is provided at <http://geodesy.unr.edu/gps/ngl.acn>.

Output station coordinates are initially in the loose frame of JPL's fiducial-free GPS orbits. Finally, the solutions are aligned by seven parameter transformation (for each day) with our custom reference frame (NA12) that co-rotates with stable North America (*Blewitt et al., 2013*). These daily transformations are publicly available at <ftp://gneiss.nbmng.unr.edu/x-files>. This alignment provides a spatial filter to suppress errors correlated at the continental scale. We deleted positions that were immediately recognizable outliers in the time series, i.e., those with values more than 20 mm from the expected position for each site based on a provisional linear model of the time series, or positions with uncertainties in any coordinate greater than 20 mm. The mean formal uncertainty in daily coordinates is 0.6 and 0.5 in the north and east directions, respectively..

Time series for stations surveyed as part of this project are shown in Appendix A. Additionally, all solutions are available as text and graphic files on <http://geodesy.unr.edu> and are browsable via a google map-driven interface or text-driven search.

#### *Correction for transient deformation from recent Earthquakes*

Tectonic studies based on GPS data rely on the measurement of steady interseismic deformation in order to relate the measurements to seismic hazard. However, recent large earthquakes deformed the network and could contaminate our analysis if these effects are not accounted for. An example is in 2010 the El Mayor-Cucapah M 7.2 earthquake occurred in northern Baja California. While this event occurred before the beginning of this project, it occurred after the time we obtained first measurements on the GPS stations. Though we expect this contribution to be small owing to the large distance between source and GPS stations we include this in the analysis because (1) some stations in our modeling domain's southwest corner are closer to epicenter and may experience significant effects and (2) the velocity gradients we are estimating are very small and could be sensitive to small perturbations. We explored the effect that this earthquake had on the time series in the vicinity of Las Vegas (which is roughly 400 km from the epicenter) by using a model for the coseismic and postseismic decay of (J. Broermann Pers. Comm. 2014) to calculate a correction for each time series. The model includes for each station an estimate of the east and north coseismic displacement and an east and north change in velocity attributable to viscoelastic relaxation following the event. Thus we can correct all measured time series using the formula

$$x(t)' = x(t) - H(t-t_{eq})*(D + dV(t-t_{eq}))$$

where  $x$  is the position as a function of time  $t$ ,  $D$  is the coseismic displacement,  $dV$  is the rate change after time of the earthquake  $t_{eq}$ , and  $H$  is the Heaviside step function. We accept that the

model is correct because we observe that it does a good job correcting for steps and apparent rate changes in the time series (Figure 2).

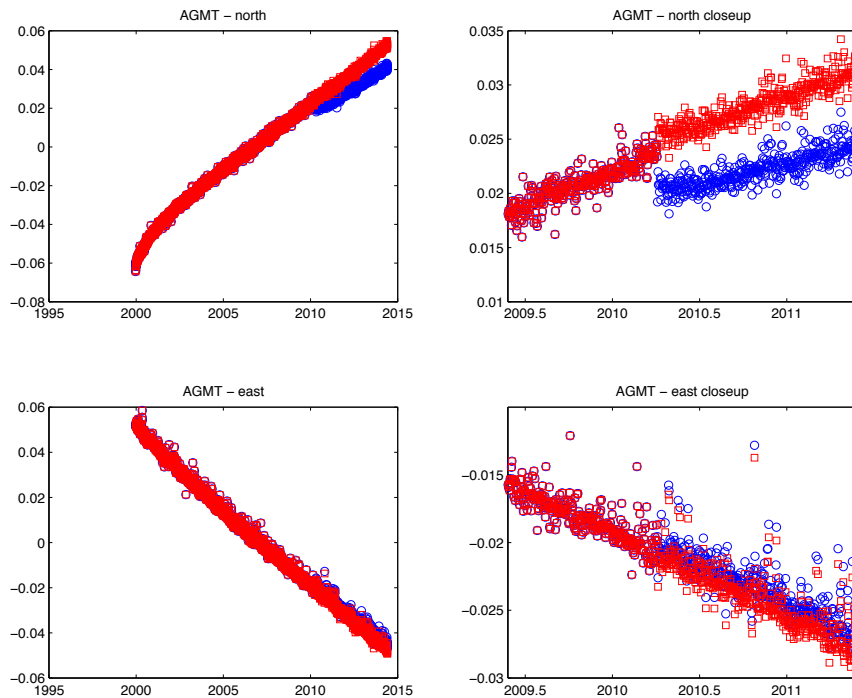


**Figure 2.** Example of the effectiveness of the correction for the 2010 earthquake on station AGMT, one of the closest stations to the epicenter used in our analysis. Left) Corrected position time series (red) for the north and east components are shown superimposed on the original time series (blue). Right) close up near time of the earthquake shows detail of how well correction recovers pre-seismic trend of the data. Vertical axis units are meters, horizontal axis is calendar years.

In addition to using the correction for the El Mayor-Cucapah earthquake, we also take steps to mitigate the effects of the 1999 M7.1 Hector Mine earthquake in southern California. For this event most of the postseismic transient was complete before the year 2002 (*Pollitz et al., 2001* and Figure 2). Since there were relatively few stations in our study area that extended this far back in time we removed data for days before time 2002.0 for these stations. While some continued effects for the earthquake may persist after 2002 and be present in our data (most of which was collected after 2007), these effects are likely smaller than the signals of interest so we ignore them for the purpose of continuum strain rate and block modeling.

## Results

### *Velocity Field*

The resulting east and north time series are used to estimate rates of motion with respect to North America (Figure 2). To estimate velocities from the position time series we only used stations that had at least 2.5 years of data. We omitted a few stations that exhibited, or are known to contain, non-tectonic signals (AZMP, AZGP, COSO, NVBR, NVCS, KGMN). For the east and north time series we calculated rates of motion with respect to North America by fitting the data with a model having intercept, slope, annual plus semiannual oscillations and step function offsets for each known equipment change event. Damping is applied to each of the terms in the linear inversion for the time series model parameters, where the terms are set to be zero with an a priori uncertainty large enough to allow the expected range of values. A priori standard deviation of velocity was set to  $10 \text{ mm yr}^{-1}$ , in intercept to 10 meters, in amplitude of annual and semiannual terms to 0.5 mm, in step sizes to 1 meter. The damping parameters are important particularly for the seasonal terms when the data sampling is sparse such as was the case for the MAGNET stations.

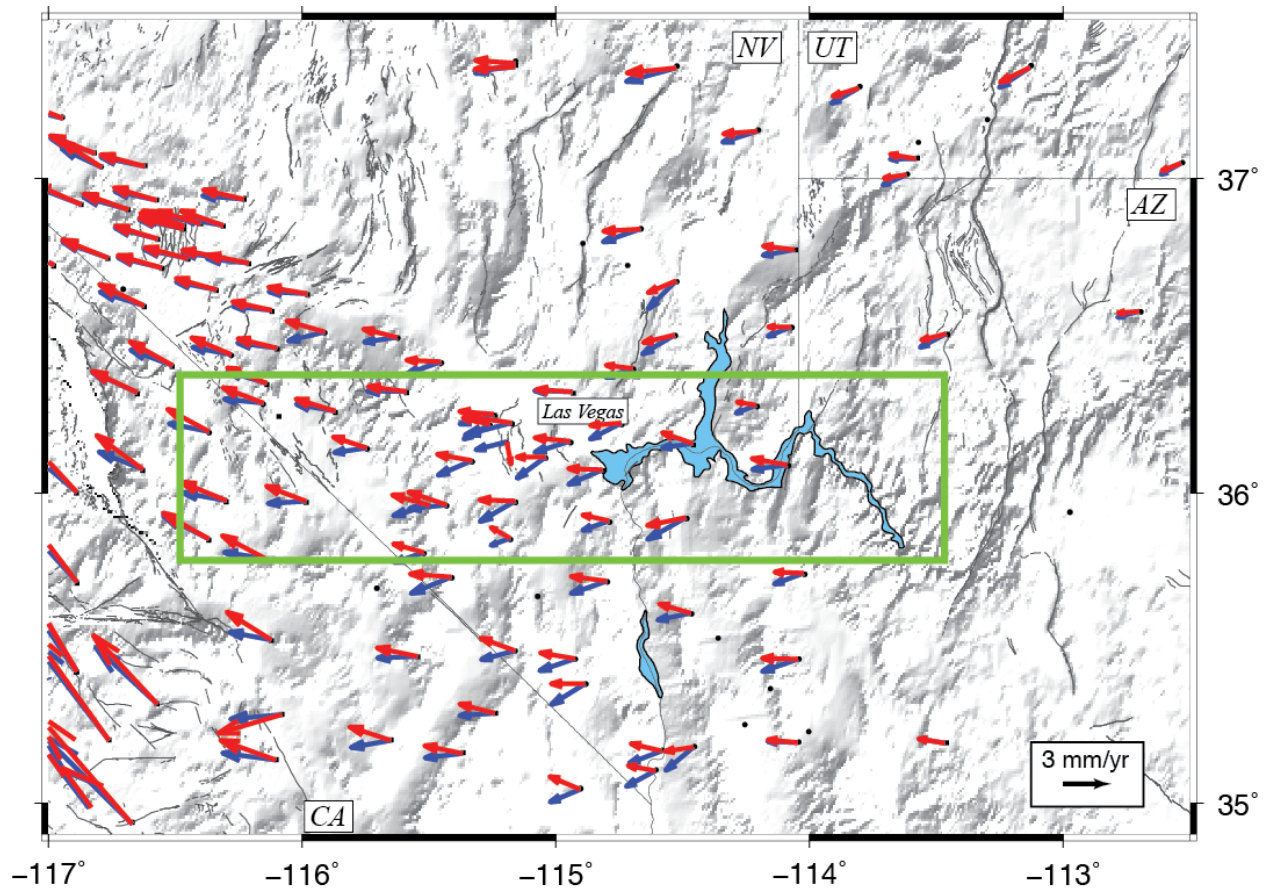


**Figure 3.** Velocities in North America reference frame NA12. Velocities from the original positions (blue) are compared to velocities that have been corrected for the effect of the 1999 Hector Mine and 2010 El Mayor-Cucapah earthquakes. Green box is location of velocity profile shown in Figure 4. GPS stations which do not yet have a velocity are shown with black dots.

The time of step events for each station is the set of unique times where a receiver or antenna equipment was changed. For each of these cases the time of the step was held fixed while the size of the step was estimated from the data. There were no equipment change events for our MAGNET stations, but there were some for nearby continuous stations. The resulting rates of motion are shown in Figure 3.

We estimated uncertainties in the rates of motion using the Hector software (*Bos et al., 2012*), which is a new method and code that estimates contributions from colored noise to the uncertainty budget using an algorithm that is faster than the CATS software we have used previously (*Williams, 2003*). In the calculations we included contributions from white and power law noise. The software estimates the relative proportion and amplitude of contribution from each noise source. The uncertainties are provided in the table of GPS velocities in Appendix A. While including colored noise generally provides larger, more realistic uncertainties, we found that many were still very low. Thus for the purpose of modeling we assigned an uncertainty floor of 0.1 mm/yr to prevent a few continuously recording sites from overly-influencing the inversion.

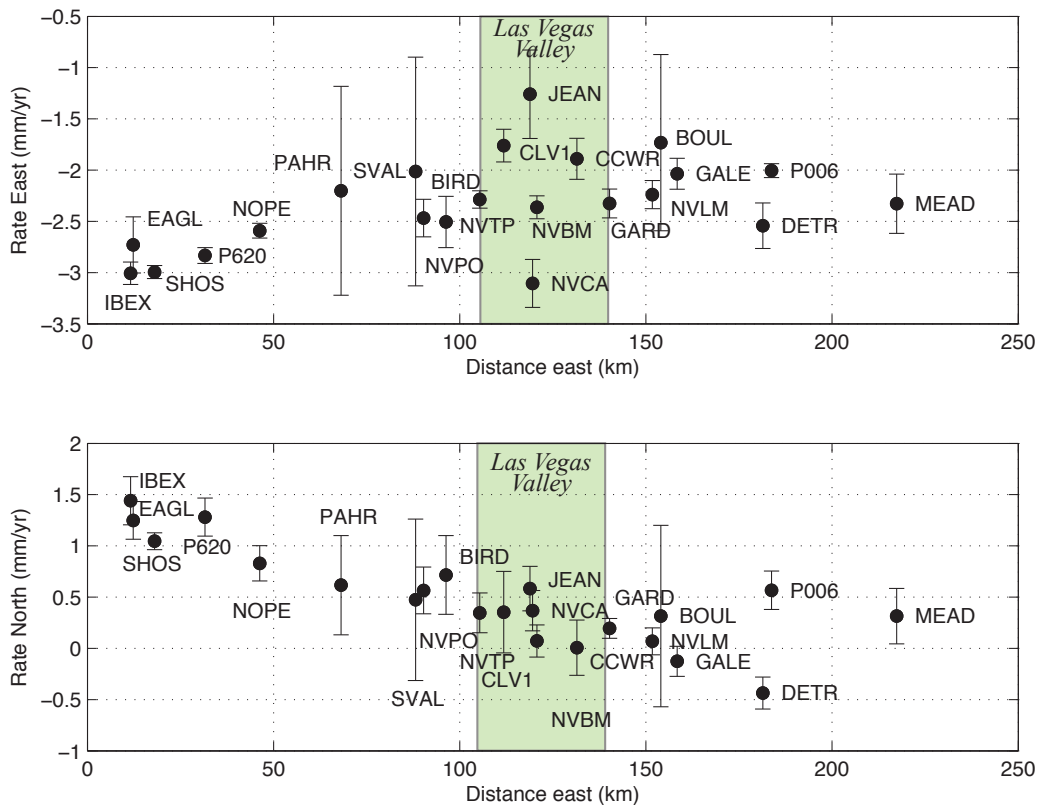


**Figure 4.** GPS velocity along and across east-west profile at latitude 36° latitude, crossing Las Vegas. Green zone shows longitudinal zone occupied by the Las Vegas Valley. Error bars are 2-sigma uncertainties.

The pattern of velocities indicates that the study area moves on average westward at 2.5 mm/yr, with west rates increasing by about 1 mm/yr across the area shown in Figure 4. The north rates also increase westward, from near zero on the east to about 1.5 mm/yr to the west. These changes in rate show the transition from slow extensional deformation in the east to more rapid transtension west of the Stateline fault merging with Southern Walker Lane/Eastern California Shear Zone on the west side of the network. We see that the correction for the recent earthquakes has a big affect on the apparent azimuth of the velocities in the south-central part of our network because 1) these stations are closer the epicenters, 2) the data at these stations tended to have been collected shortly after the event, 3) the rates are lower and hence more sensitive to small perturbations from the earthquakes and 4) this zone lies in the northeast quadrant of the deformation zones where gradients in coseismic and postseismic response tend to be largest (e.g. *Freed et al.*, 2007; *Hammond et al.*, 2010).

Profiles (Figure 4) centered on Las Vegas Valley show about 2 mm/yr over 200 km, or  $\sim 10$  nanostrains/yr of deformation. This is over twice as large as strain rates in northeast Nevada where the Wells NV, M6.0 occurred (*Hammond et al.*, 2014), and about one order of magnitude less than the mean strain rates typically observed in the Walker Lane Belt.

### *Strain Rate Map*

We used the observed horizontal velocity field to determine a spatially-continuous strain rate model, but, following *Kreemer et al.* (2014), multiplied the standard deviations with a factor of 2. For this purpose we considered the area from 118°W-112°W and 34°N-39°N. We fixed the eastern edge of this box and approximated it as stable North America (the reference of the GPS velocities). This area was divided into grid cells of 0.25° (longitude) and 0.2° (latitude) in dimension. We then used the method of *Haines and Holt* (1993) which uses bi-cubic splines to obtain a continuous velocity gradient tensor field. Because this method relies on an *a priori* strain rate variances for each cell, we employ a two-step empirical Bayesian approach.

In the first step we set the *a priori* strain rate standard deviations to  $10^{-9}$  yr<sup>-1</sup> and zero covariances (i.e., assumed isotropy). In the second step, we took the modeled strain rate field from the first step and used it to constrain the *a priori* standard deviations. For this, we did not take the style or covariances but set the *a priori* standard deviation equal to the second invariant of the tensor modeled in step 1. In the first step the weighted RMS fit to the data is 14.1 and in step 2 it is 1.2.

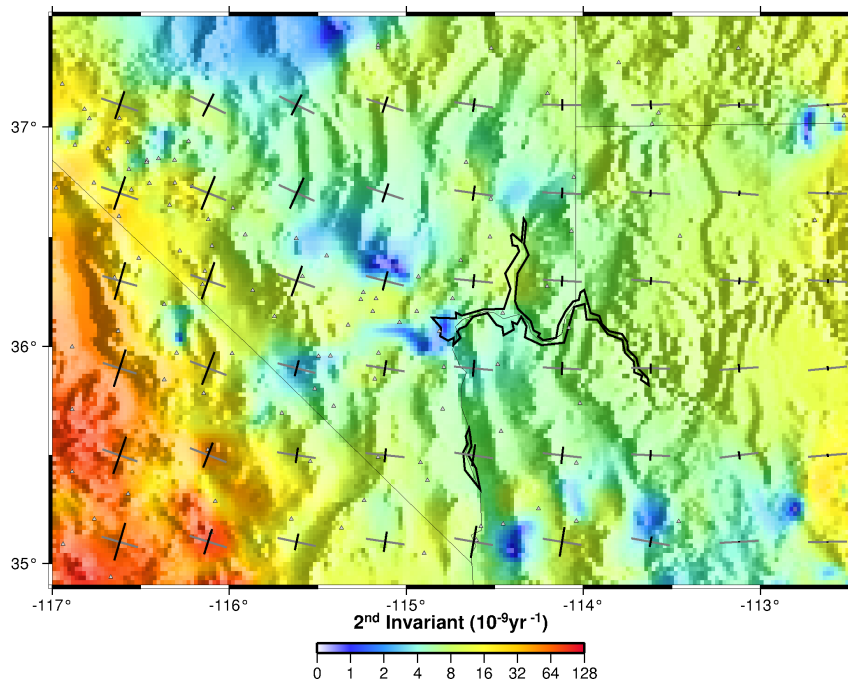


**Figure 5.** Strain rate map derived from GPS velocities. Color shows the second-invariant of the strain rate model. Note the non-linear scale. Also shown are principal axes with the grey and black bars indicating the direction and relative amplitude of the extensional and contractional principal strain rates, respectively. Each pair is scaled to the largest value. The grey triangles are the locations of the GPS stations.

In Figure 5 we show the second-invariant of the strain rate model. The figure also shows the principal strain rate axes. The style of strain changes from unilateral EW extension in the east to shear strain along a NW-SE direction in the west. Strain rates are relatively high in the east ( $10\text{-}20 \times 10^{-9} \text{ yr}^{-1}$ ), but this may be an artifact of fixing the zero-reference to  $112^\circ\text{E}$ . In the central part of the model, across Las Vegas Valley, strain rates vary spatially but are everywhere  $< 10^{-8} \text{ yr}^{-1}$ . Strain rates reach  $10^{-7} \text{ yr}^{-1}$  in the Eastern California Shear Zone.

### *Block Model*

Our model was constructed to estimate slip rates on the major active faults in and around southern Nevada (Figure 6). Block boundaries were drawn to coincide with active faults and given provisional dips of either  $50^\circ$  or  $80^\circ$  depending on whether the fault was thought to be predominately normal or strike slip. We used the USGS Quaternary Fault and Fold Database (QFFD) which documents the geometry and activity of faults to guide the definition of the block boundaries. Owing to the discontinuous nature of faults in this area, this exercise has some subjectivity since this modeling strategy requires blocks to be contiguous so they can move independently, thus decisions often had to be made on how to join faults into contiguous boundaries. Our model is intended to quantify the budget of slip across southern Nevada and infer the style of deformation that is demanded by the GPS data. Our model has 19 blocks, constrained by 108 velocities (Appendix A).

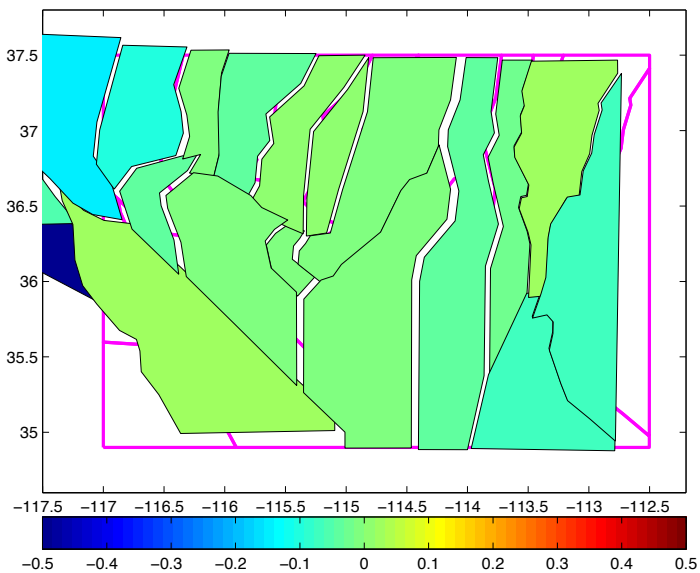
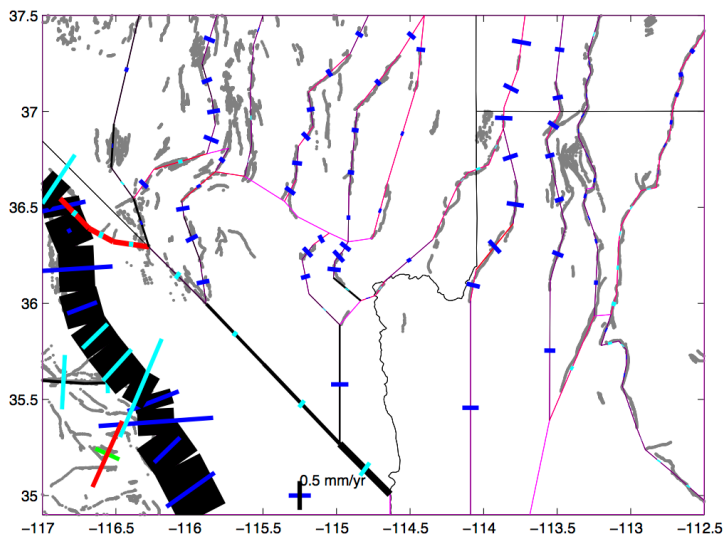
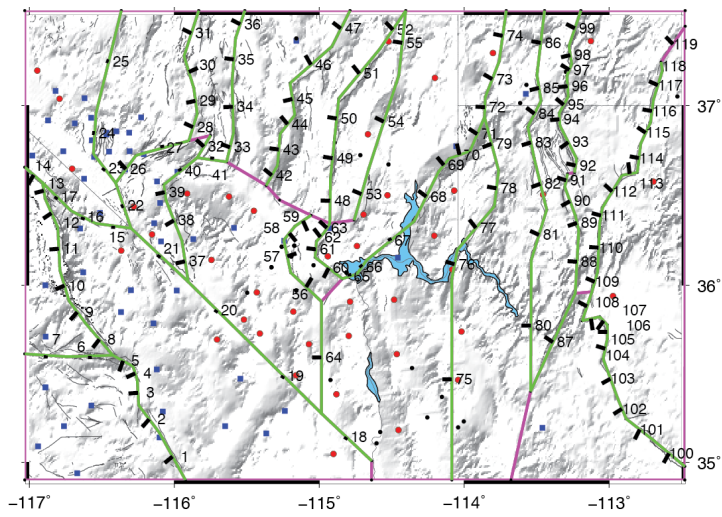


**Figure 6.** Results of block modeling of deformation across southern Nevada, eastern California and western Arizona. Top) Block boundaries and faults are shown with fault numbers, and black tags that indicate dip of fault (longer tags are shallower, no tag is a vertical fault). Middle) Slip rates estimated in the model, blue=normal rate indicated by length, cyan=thrust rate indicated by length, black=dextral rate indicated by thickness, red=sinistral rate indicated by thickness. Bottom) Diagram indicating map view pattern of model block motions. Color scale indicates vertical axis spin rate in degrees per million years.

We solved for block motions and slip rates in a simultaneous inversion using a block modeling method that has been used previously to model tectonic deformation in the Great Basin (*Hammond et al.*, 2007; 2011). Because not all blocks have their motion constrained by GPS data we employ a regularization that minimizes the slip rates and vertical axis spin rates. This causes unconstrained blocks (with zero GPS stations, 2 in the model) or poorly constrained blocks (with one GPS station, 3 in the model) to move in a way that minimizes the misfit with adjacent blocks. This damping constraint results in a smoother model compared to an unconstrained model. We performed an outlier detection and removal step in which we excluded three more of the GPS velocities (stations AZLH, AZGV, LVWD). After this exclusion the RMS misfit between the GPS velocity data and the model predictions is 0.33 (0.35) mm/yr, indicating a close fit to the data.

The resulting model shows that normal slip is distributed across southern Nevada from the Colorado Plateau in western Arizona to eastern California. We do not find any single fault system that dominates over the others or any normal slip rate outside the Walker Lane/ECSZ that is greater than 0.4 mm/yr, though there are variations from 0.02 to 0.4 mm/yr normal rate (projected to the horizontal). The Stateline Fault has a dextral slip rate  $0.8 \pm 0.4$  mm/yr, significantly lower than the geological rate inferred by (*Guest et al.*, 2007).

Faults very near the population center of Las Vegas (e.g. the Eglinton Fault and Frenchman Mountain Fault) slip near 0.2 mm/yr in our model. This is reasonable given that 1) both of these faults have their rates listed as “<0.2 mm/yr” in the QFFD (*USGS and CGS, USGS and NBMG, USGS and AGS*, 2014), and 2) this valley sits inside a 200 km-wide zone accommodating  $\sim 2$  mm/yr over 10 faults systems as noted above. However, surface deformation associated with hydrological pumping within the Las Vegas Valley perturbs the surface in ways that are not completely understood, reducing our ability to partition strain onto individual faults within the basin. Slip rates averaged across groups of individual faults segments, which we call trains, are provided in Table 1.

## Conclusions

We measured 24 MAGNET GPS stations which now have a minimum of 7 years between their first and last observation. From these measurements we estimated the velocity of crustal motion, accounting for deformation from the 2010 El Mayor-Cucapah and 1999 Hector Mine earthquakes that caused detectable co- and post seismic deformation in the network. From this new velocity field we generated a horizontal tensor strain rate map and a crustal block motion model to estimate slip rates on active faults in area revealing active deformation distributed across southern Nevada, eastern California and western Arizona. We find that  $\sim 2$  mm/yr of extensional strain is distributed over about  $\sim 200$  km centered on Las Vegas, giving a strain accumulation rate of near  $10 \times 10^{-9} \text{ yr}^{-1}$ , which is intermediate between that of the Walker Lane and eastern Nevada.

Results of block modeling suggest that faults near the population center of Las Vegas

(e.g. the Eglinton Fault and Frenchman Mountain Fault) have slip rates near 0.2 mm/yr. This is reasonable given that 1) both of these faults have their rates based on geologic studies listed as <0.2 mm/yr in the QFFD, and 2) this valley sits inside a 200 km-wide zone accommodating ~2 mm/yr over roughly 10 normal fault systems. The Stateline Fault has a dextral slip rate  $0.8 \pm 0.4$  mm/yr, significantly lower than the geological rate. We do not find any single fault system across southern Nevada that dominates over the others (i.e. has a much higher slip rate) or any normal slip rate outside the Walker Lane/ECSZ that is greater than 0.4 mm/yr, though there are variations from 0.02 to 0.4 mm/yr (projected to the horizontal).

**Table 1.** Fault slip rates from block model. Fault numbers are given in Figure 6.

Fault Train Number	A Fault in Train	Number of Faults in Train	Strike Slip (mm/yr)	Normal Horizontal (mm/yr)
1	1	5	-4.70+/-0.89	-0.74+/-1.86
2	6	2	-0.29+/-0.47	0.81+/-0.58
3	8	6	-4.29+/-0.50	-0.35+/-1.10
4	14	1	-3.49+/-0.46	1.85+/-0.43
5	15	3	0.60+/-0.33	0.14+/-0.16
6	18	1	-0.81+/-0.38	0.34+/-0.19
7	19	2	-0.43+/-0.36	0.14+/-0.18
8	21	1	-0.11+/-0.36	0.16+/-0.14
9	22	1	-0.24+/-0.21	-0.04+/-0.16
10	23	3	-0.15+/-0.21	-0.03+/-0.11
11	26	2	0.05+/-0.21	-0.07+/-0.27
12	28	4	-0.05+/-0.21	-0.29+/-0.41
13	32	1	-0.01+/-0.22	-0.14+/-0.41
14	33	4	-0.05+/-0.21	0.07+/-0.46
15	37	4	-0.04+/-0.23	-0.27+/-0.19
16	41	1	0.09+/-0.24	0.01+/-0.28
17	42	6	-0.02+/-0.21	-0.20+/-0.39
18	48	5	-0.02+/-0.21	-0.18+/-0.45
19	53	3	0.02+/-0.21	-0.12+/-0.44
20	56	4	-0.03+/-0.22	-0.22+/-0.35
21	60	4	-0.10+/-0.22	-0.18+/-0.34
22	64	1	-0.19+/-0.21	-0.38+/-0.36
23	65	7	0.02+/-0.20	0.02+/-0.17
24	72	3	0.03+/-0.21	-0.42+/-0.42
25	75	5	0.01+/-0.20	-0.36+/-0.38
26	80	7	-0.03+/-0.20	-0.14+/-0.39
27	87	1	0.04+/-0.22	0.05+/-0.50
28	88	12	-0.02+/-0.20	-0.04+/-0.36
29	100	9	-0.03+/-0.20	0.02+/-0.30
30	109	11	0.02+/-0.20	-0.08+/-0.32

## Papers and Presentations

- Blewitt, G., C. Kreemer, W.C. Hammond, J. Goldfarb, 2013, Terrestrial reference frame NA12 for crustal deformation studies in North America, *J. Geodynamics*, 72, pp. 11-24, ISSN 0264-3707, <http://dx.doi.org/10.1016/j.jog.2013.08.004>.
- Bormann, J., W.C. Hammond, G. Blewitt, C. Kreemer, S. Jha, A synoptic model of fault slip rates in the Eastern California Shear Zone and Walker Lane from GPS velocities for seismic hazard studies, SSA Annual Meeting, Salt Lake City, Utah, April 17-19, 2013.
- Hammond, W.C., G. Blewitt, C. Kreemer, 2014, Steady contemporary deformation of the central Basin and Range Province, western United States, *J. Geophys. Res.*, 10.1002/2014JB011145.
- Hammond, W.C., J.M. Bormann, G. Blewitt, C. Kreemer, 2013, A province-scale block model of Walker Lane and western Basin and Range crustal deformation constrained by GPS observations, Fall AGU, G43C-08, San Francisco, CA, Dec 9-13, 2013, [INVITED].
- Hammond, W.C. J. Bormann, G. Blewitt, C. Kreemer, 2013, Walker Lane and western Basin and Range transtension and rotation rates from GPS observations, continuum and block models, GSA Annual Meeting Session No. 85 T205, Denver CO, Oct. 27-30, 2013 [INVITED].
- Kreemer, C., Blewitt, G., and Hammond, W.C., 2013, The GPS velocity field in the western U.S. And what it tells us about earthquakes, seismic hazard, and driving forces, Abstract S23C-05, Fall Meeting, AGU, San Francisco.
- Kreemer, C., Blewitt, G., Hammond, W.C., Broermann, J., and Bennett, R.A., 2013, Improved seismic hazard assessment for the Colorado Plateau region from new geodetic, data, SSA Annual Meeting, Salt Lake City.
- Petersen, M.D., Y. Zeng, K.M. Haller, R. McCaffrey, W.C. Hammond, P. Bird, M Moschetti, Z. Shen, J. Bormann, and W. Thatcher, 2014, Geodesy- and geology-based slip-rate models for the Western United States (excluding California) national seismic hazard maps: U.S. Geological Survey Open-File Report 2013–1293, 80 p., <http://dx.doi.org/10.3133/ofr20131293>.

## References

- Bertiger, W., Shailen D., B Haines, N Harvey, A.W. Moore, S. Owen, and J P. Weiss, 2010, Single Receiver Phase Ambiguity Resolution with GPS Data, *Journal of Geodesy* 84, no. 5 327–37. doi: 10.1007/s00190-010-0371-9.
- Blewitt, G., 1989, Carrier Phase Ambiguity Resolution for the Global Positioning System Applied to Geodetic Baselines up to 2000 Km, *Journal of Geophysical Research*, 94,10,187–10,283.
- Blewitt, G., C. Kreemer, W.C. Hammond, J. Goldfarb, 2013, Terrestrial reference frame NA12 for crustal deformation studies in North America, *J. Geodynamics*, 72, pp. 11-24, ISSN 0264-3707, doi:10.1016/j.jog.2013.08.004.
- Boehm, J., A. Niell, P. Tregoning, and H. Schuh, 2006, Global Mapping Function (GMF): A New Empirical Mapping Function Based on Numerical Weather Model Data, *Geophysical Research Letters* 33, no. 7.
- Bos, M.S., R.M.S. Fernandes, S.D.P. Williams, and L. Bastos, 2013, Fast Error Analysis of Continuous GNSS Observations with Missing Data, *Journal of Geodesy* 87, no. 4, 351–60. doi:10.1007/s00190-012-0605-0.
- Faulds, J. E., and Henry, C. D., 2008, Tectonic Influences on the Spatial and Temporal Evolution of the Walker Lane: An Incipient Transform Fault along the Evolving Pacific – North American Plate Boundary, in Spencer, J.E., and Titley, S.R., eds., *Ores and Orogenesis: Circum-Pacific Tectonics, Geologic Evolution, and Ore Deposits*, 437–70, Arizona Geological Society Digest 22, n.d.
- Freed, A. M., R. Burgmann, and T. Herring, 2007, Far-Reaching Transient Motions after Mojave Earthquakes Require Broad Mantle Flow beneath a Strong Crust, *Geophysical Research Letters* 34, no. 19 (2007). doi://000250045200004.
- Guest, B, N Niemi, and B. Wernicke, 2007, Stateline Fault System: A New Component of the Miocene-Quaternary Eastern California Shear Zone, *GSA Bulletin* 119, no. 11/12, 1337–47, doi: 10.1130B26138.1.

- Haines, A. J., and W. E. Holt, 1993, A procedure for obtaining the complete horizontal motions within zones of distributed deformation from the inversion of strain rate data, *J. Geophys. Res.*, 98(B7), 12057–12082, doi:10.1029/93JB00892.
- Hammond, W. C., and W. Thatcher., 2007, Crustal Deformation across the Sierra Nevada, Northern Walker Lane, Basin and Range Transition, Western United States Measured with GPS, 2000-2004, *Journal of Geophysical Research* 112, B05411, doi:10.1029/2006JB004625.
- Hammond, W. C., C. Kreemer, G. Blewitt, and H.-P. Plag, Effect of Viscoelastic Postseismic Relaxation on Estimates of Interseismic Crustal Strain Accumulation at Yucca Mountain, Nevada, *Geophysical Research Letters* 37, L06307, doi:10.1029/2010GL042795.
- Hammond, William C., G. Blewitt, and C. Kreemer, 2011, Block Modeling of Crustal Deformation of the Northern Walker Lane and Basin and Range from GPS Velocities, *Journal of Geophysical Research: Solid Earth*, 116, no. B4, B04402. doi:10.1029/2010JB007817.
- Hammond, W.C., G. Blewitt, C. Kreemer, 2014, Steady contemporary deformation of the central Basin and Range Province, western United States, *J. Geophys. Res.*, doi:10.1002/2014JB011145.
- Kreemer, C, G. Blewitt, W.C. Hammond, 2010, Evidence for an Active Shear Zone in Southern Nevada Linking the Wasatch Fault to the Eastern California Shear Zone, *Geology* 38, no. 5, 475–78.
- Kreemer, C., G. Blewitt, and E.C. Klein, 2014, A geodetic plate motion and global strain rate model, *Geophys. Geochem. Geosys.*, in revision.
- Petersen et al., 2008, Documentation for the 2008 Update of the United States National Seismic Hazard Maps, USGS Open-File Report 2008–1128.
- Pollitz, F. F., C Wicks, and W. Thatcher, Mantle Flow Beneath a Continental Strike Slip Fault: Postseismic Deformation After the 1999 Hector Mine Earthquake, *Science* 293,1814–18.
- Scherneck, H. G.. 1991, A Parametrized Solid Earth Tide Model and Ocean Tide Loading Effects for Global Geodetic Base-Line Measurements, *Geophysical Journal International*, 106, no. 3, 677–94.
- U.S. Geological Survey and Arizona Geological Survey, 2014, Quaternary Fault and Fold Database for the United States, 2014, <http://earthquake.usgs.gov/regional/qfaults/>.
- U.S. Geological Survey and California Geological Survey, Quaternary Fault and Fold Database for the United States, 2014, <http://earthquake.usgs.gov/regional/qfaults/>.
- U.S. Geological Survey and Nevada Bureau of Mines and Geology. Quaternary Fault and Fold Database for the United States, 2006, <http://earthquake.usgs.gov/regional/qfaults/>.
- Williams, S. P. D., 2003, The Effect of Coloured Noise on the Uncertainties of Rates Estimated from Geodetic Time Series, *Journal of Geodesy* 76, 483–94.
- Zumberge, James, M.B. Heflin, D.C. Jefferson, M.M. Watkins, and Frank H. Webb, 1997, Precise Point Positioning for the Efficient and Robust Analysis of GPS Data from Large Networks, *Journal of Geophysical Research* 102, no. B3, 5005–17.

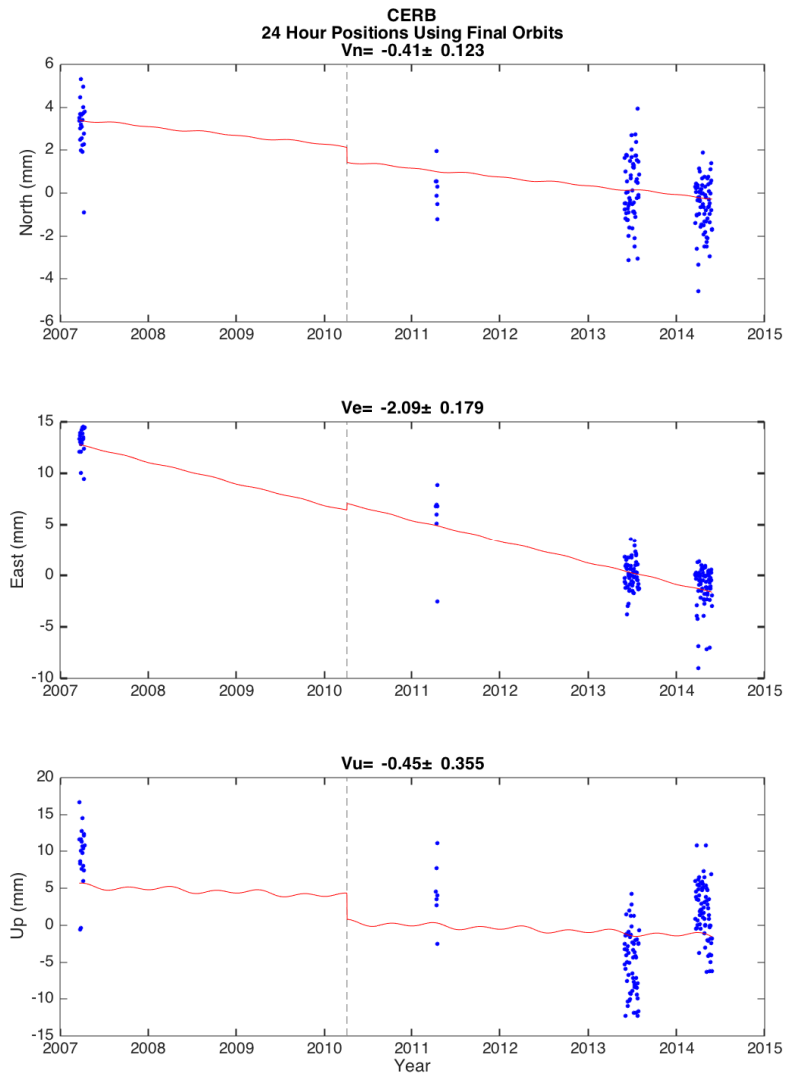
**Appendix A.** Velocities corrected for 2010 El Major-Cucapah and 1999 Hector Mine earthquakes. This table includes velocities for all stations with sufficient data inside the area shown in Figure 1 that are processed by the Nevada Geodetic Laboratory and used for the modeling. Uncertainties are estimated using the Hector software (*Bos et al., 2012*), with uncertainty floor of 0.1 mm/yr imposed.

<b>Station</b>	<b>Latitude</b>	<b>Longitude</b>	<b>Vn</b>	$\sigma_{Vn}$	<b>Ve</b>	$\sigma_{Ve}$	<b>Duration</b>
	<b>(degrees)</b>	<b>(degrees)</b>	<b>(mm/yr)</b>	<b>(mm/yr)</b>	<b>(mm/yr)</b>	<b>(mm/yr)</b>	<b>(years)</b>
ALAM	37.358	-115.158	-0.12	0.10	-2.65	0.10	11.4
APEX	36.319	-114.932	0.12	0.10	-2.38	0.10	10.2
ASHM	36.346	-116.139	0.83	0.10	-2.60	0.10	5.0
AZBH	35.107	-114.605	0.27	0.10	-1.78	0.19	5.8
AZFM	34.852	-114.595	0.51	0.11	-1.85	0.10	5.6
AZGV	35.254	-114.254	2.31	0.39	-0.80	0.46	3.7
AZMP	35.371	-114.154	-1.96	0.67	-27.30	1.00	4.9
BATM	36.403	-116.512	1.28	0.13	-2.81	0.10	4.9
BEAT	37.040	-116.621	0.62	0.10	-2.90	0.10	11.6
BIRD	35.958	-115.429	0.70	0.19	-2.51	0.13	6.9
BKAP	35.287	-116.080	-0.99	0.10	-4.18	0.10	13.5
BOUL	35.907	-114.788	0.31	0.44	-1.73	0.43	6.3
BULL	36.918	-116.872	1.10	0.10	-3.10	0.10	12.1
BUST	36.745	-116.451	0.59	0.10	-2.85	0.10	10.9
CCWR	36.110	-115.039	0.00	0.13	-1.89	0.10	6.1
CDMT	34.829	-116.336	2.17	0.10	-5.95	0.10	13.6
CERB	35.465	-114.041	0.04	0.34	-2.35	0.43	6.4
CHLO	36.747	-116.766	0.99	0.10	-3.02	0.10	11.7
CLV1	36.215	-115.258	0.34	0.20	-1.76	0.10	5.9
CRAM	37.081	-116.818	0.95	0.10	-2.94	0.10	4.9
CRAT	36.808	-116.569	0.69	0.10	-2.80	0.10	10.8
DETR	35.917	-114.484	-0.43	0.10	-2.54	0.11	6.3
DEVL	36.438	-116.280	0.91	0.13	-2.61	0.10	8.2
EAGL	36.192	-116.367	1.20	0.10	-2.75	0.14	8.1
ELGI	37.355	-114.522	-0.27	0.37	-3.25	0.66	3.0
GALE	36.219	-114.739	-0.13	0.10	-2.04	0.10	6.4
GARD	36.161	-114.941	0.19	0.10	-2.33	0.10	6.4
GOAT	36.527	-114.068	0.00	0.21	-1.50	0.32	6.3
GOL2	35.425	-116.889	6.51	0.10	-4.74	0.10	18.4
GOLD	35.425	-116.889	6.43	0.10	-4.77	0.10	18.4
GUNL	37.290	-113.802	-0.44	0.24	-1.71	0.22	3.0
HELL	36.724	-116.979	1.49	0.10	-3.36	0.10	3.5
HIGH	36.283	-116.153	0.82	0.13	-2.65	0.12	8.5
HOME	35.048	-114.901	0.69	0.19	-2.01	0.18	6.7
HUAL	35.739	-114.019	0.06	0.18	-1.91	0.27	6.4
HURR	37.064	-113.575	0.24	0.10	-1.71	0.10	6.2
HW95	37.193	-116.945	1.10	0.10	-3.37	0.10	7.7
IBEX	35.848	-116.368	1.39	0.12	-3.03	0.10	4.2
IVAN	35.727	-115.410	0.16	0.21	-2.70	0.28	6.6
JEAN	35.851	-115.178	0.58	0.11	-1.26	0.22	6.4
JOHN	36.459	-116.099	0.50	0.10	-2.58	0.10	12.0
JONE	37.152	-114.202	-0.14	0.10	-2.23	0.10	3.2
KAYO	35.195	-113.461	0.24	0.10	-1.73	0.10	5.3
KEMP	35.612	-114.465	0.49	0.12	-2.07	0.13	6.5
KING	35.197	-114.041	0.16	0.11	-1.97	0.11	12.3
LICE	36.857	-116.401	0.68	0.10	-2.78	0.10	4.4

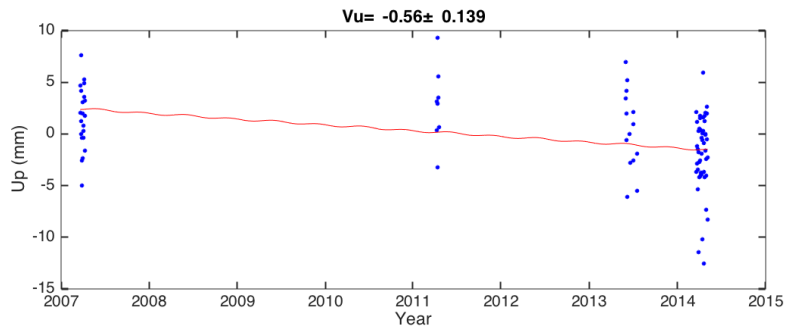
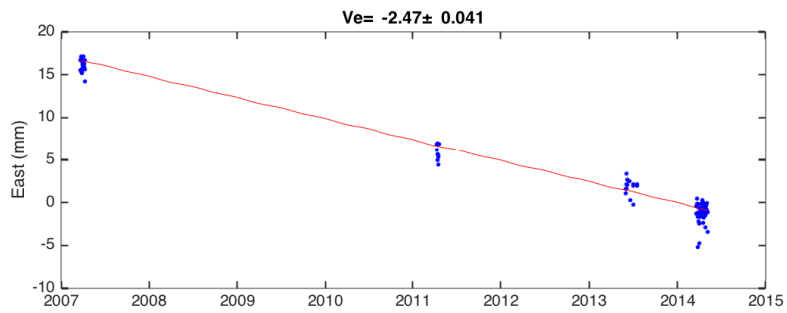
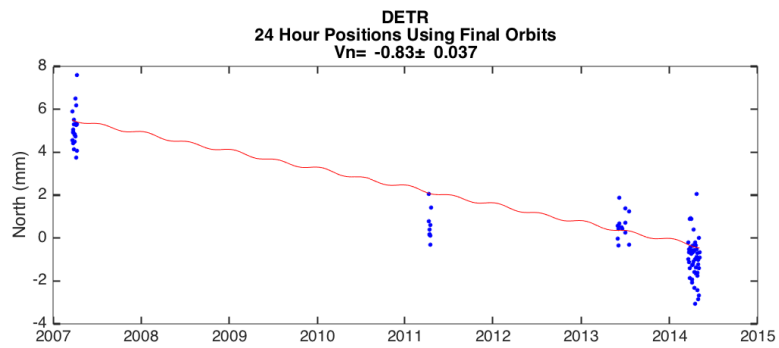
Station	Latitude	Longitude	Vn	$\sigma_{Vn}$	Ve	$\sigma_{Ve}$	Duration
	(degrees)	(degrees)	(mm/yr)	(mm/yr)	(mm/yr)	(mm/yr)	(years)
LITT	36.746	-116.308	0.43	0.10	-2.74	0.10	11.0
LNMT	35.090	-116.940	7.95	0.10	-7.07	0.10	13.4
LVWD	36.159	-115.191	-1.20	0.29	0.29	0.16	6.7
MEAD	36.086	-114.083	0.33	0.13	-2.33	0.14	6.4
MERC	36.633	-115.979	0.34	0.10	-2.55	0.10	11.9
MUDD	36.394	-114.694	0.18	0.15	-1.75	0.15	6.5
NELS	35.714	-114.796	0.25	0.24	-2.37	0.25	6.5
NEVA	36.850	-116.310	0.80	0.11	-2.81	0.10	4.4
NOPE	35.969	-115.985	0.80	0.10	-2.60	0.10	7.3
NVAL	37.370	-115.159	0.15	0.17	-2.62	0.14	5.6
NVBM	35.970	-115.158	0.06	0.10	-2.36	0.10	6.6
NVCA	36.220	-115.172	0.36	0.10	-3.11	0.12	6.8
NVGL	36.673	-114.523	-0.63	0.16	-1.84	0.11	4.9
NVLA	35.171	-114.580	0.39	0.13	-2.02	0.11	6.1
NVLM	36.070	-114.813	0.07	0.10	-2.24	0.10	7.9
NVPO	35.956	-115.496	0.55	0.11	-2.47	0.10	7.3
NVSL	35.466	-114.921	0.31	0.17	-2.29	0.10	6.6
NVTP	36.099	-115.329	0.33	0.10	-2.29	0.10	6.6
NYOR	35.491	-115.159	0.68	0.17	-2.25	0.19	6.3
OASI	37.037	-116.791	1.42	0.10	-2.71	0.10	7.7
P006	36.154	-114.457	0.57	0.10	-2.00	0.10	6.7
P462	36.071	-116.629	1.81	0.10	-3.05	0.10	7.5
P596	35.998	-116.890	3.52	0.10	-4.03	0.10	7.3
P597	35.711	-116.888	4.89	0.11	-4.64	0.10	7.3
P604	34.937	-116.671	5.93	0.10	-6.30	0.10	6.1
P611	35.205	-115.650	0.72	0.10	-2.71	0.10	8.3
P615	35.205	-116.763	6.07	0.10	-5.36	0.10	8.0
P617	35.321	-116.572	3.66	0.10	-4.23	0.10	8.0
P618	35.142	-116.104	1.05	0.10	-3.63	0.10	8.4
P619	35.526	-116.122	1.49	0.10	-2.92	0.10	5.8
P620	35.785	-116.145	1.24	0.10	-2.85	0.10	6.2
P621	35.473	-115.544	0.46	0.10	-2.67	0.10	8.7
P622	35.163	-115.366	0.41	0.10	-2.49	0.10	8.6
P625	34.844	-114.965	0.66	0.10	-2.09	0.10	6.8
P626	35.291	-115.238	0.49	0.10	-2.32	0.10	8.6
PAHR	36.139	-115.745	0.59	0.24	-2.21	0.51	6.5
PERL	36.902	-116.686	0.84	0.10	-2.94	0.10	12.3
PIUT	35.385	-114.882	0.00	0.25	-2.24	0.25	6.5
POIN	36.580	-116.120	0.46	0.10	-2.57	0.10	12.0
RELA	36.715	-116.554	0.67	0.10	-2.88	0.10	10.8
REP2	36.840	-116.468	0.79	0.10	-2.80	0.10	4.4
REP3	36.841	-116.468	0.82	0.10	-2.83	0.10	4.4
REP4	36.849	-116.466	0.82	0.12	-2.70	0.10	4.4
REPO	36.840	-116.468	0.59	0.10	-2.91	0.10	10.8
RIDG	36.493	-115.623	0.44	0.64	-2.24	1.58	6.5
ROXY	36.840	-114.664	-0.12	0.14	-2.42	0.10	3.1
RUMP	36.257	-115.868	0.65	0.12	-2.59	0.10	5.2
RYAN	36.316	-116.650	1.15	0.10	-2.98	0.10	11.4
SHIV	36.505	-113.456	-0.34	0.12	-1.62	0.13	3.2
SHOS	35.971	-116.299	1.00	0.10	-3.01	0.10	15.2
SKUL	36.730	-116.211	0.43	0.10	-2.70	0.10	11.7
SMYC	36.320	-115.587	0.27	0.10	-2.52	0.10	12.0
STIR	36.510	-115.910	0.59	0.26	-2.52	0.13	6.5
STRI	36.645	-116.338	0.61	0.10	-2.67	0.10	12.1

<b>Station</b>	<b>Latitude</b>	<b>Longitude</b>	<b>V<sub>n</sub></b>	<b><math>\sigma_{V_n}</math></b>	<b>V<sub>e</sub></b>	<b><math>\sigma_{V_e}</math></b>	<b>Duration</b>
	<b>(degrees)</b>	<b>(degrees)</b>	<b>(mm/yr)</b>	<b>(mm/yr)</b>	<b>(mm/yr)</b>	<b>(mm/yr)</b>	<b>(years)</b>
STRK	36.415	-115.451	0.08	0.23	-2.27	0.15	6.6
SUNS	36.577	-112.693	-0.09	0.11	-1.38	0.10	3.2
SVAL	35.806	-115.518	0.46	0.39	-2.02	0.56	6.5
TATE	36.932	-116.574	0.66	0.10	-2.80	0.10	12.1
THUM	35.183	-114.454	-0.23	0.19	-1.86	0.15	6.2
TIVA	36.935	-116.230	0.50	0.10	-2.67	0.10	15.2
TRAM	36.276	-114.206	0.18	0.17	-1.25	0.16	6.4
TROY	34.839	-116.531	4.61	0.10	-6.93	0.10	9.8
UNR1	36.247	-115.243	0.16	0.10	-2.26	0.10	11.6
UNR2	36.773	-114.054	0.20	0.15	-2.07	0.15	11.1
UTKA	37.050	-112.528	-0.39	0.18	-1.27	0.20	3.8
UTSG	37.013	-113.613	-0.18	0.18	-1.48	0.15	3.8
VFSP	36.501	-114.529	-0.41	0.26	-2.06	0.15	3.1
VONS	36.594	-116.623	1.14	0.13	-2.97	0.10	4.9
ZION	37.356	-113.125	-0.77	0.18	-1.95	0.10	3.2

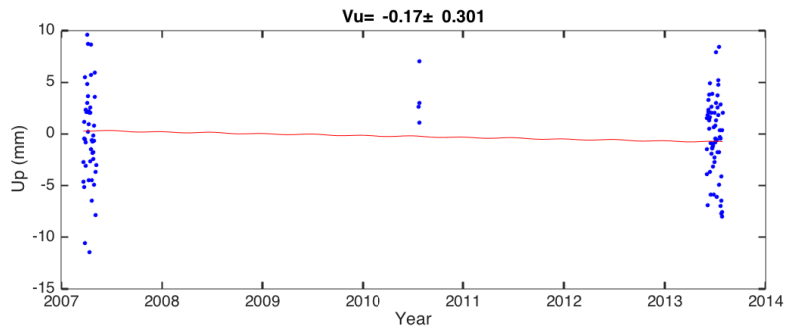
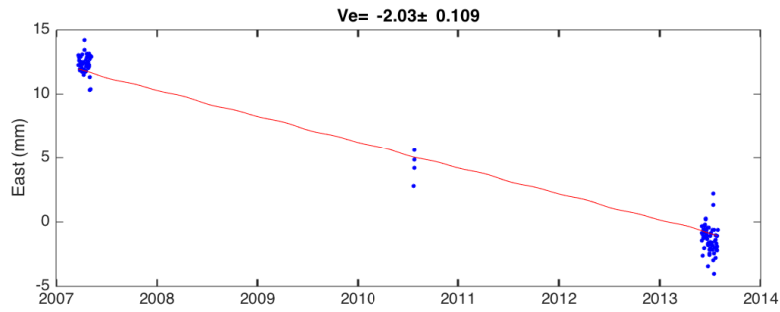
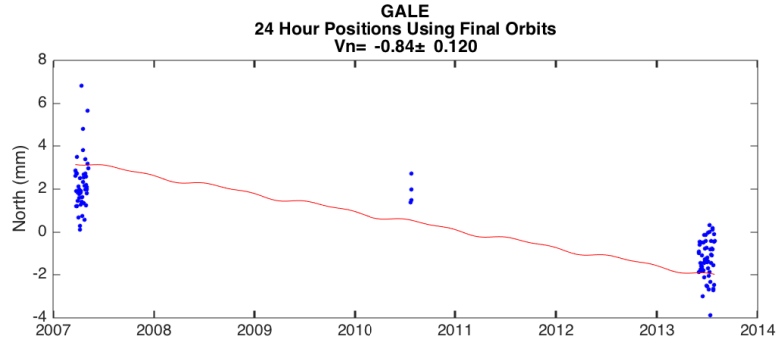
**Appendix B.** Plots of GPS position time series. Note that these figures are automatically generated and thus the rates shown are not the final rates that include correction for earthquakes. and the discontinuities do not have the same amplitude as those used in the correction. Red line indicates time series model estimated for graphic presentation of time series.



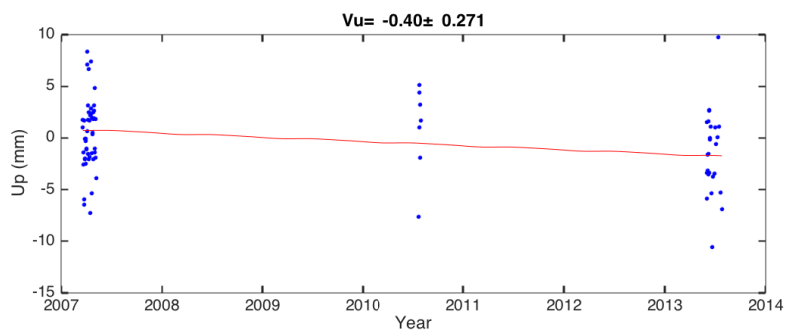
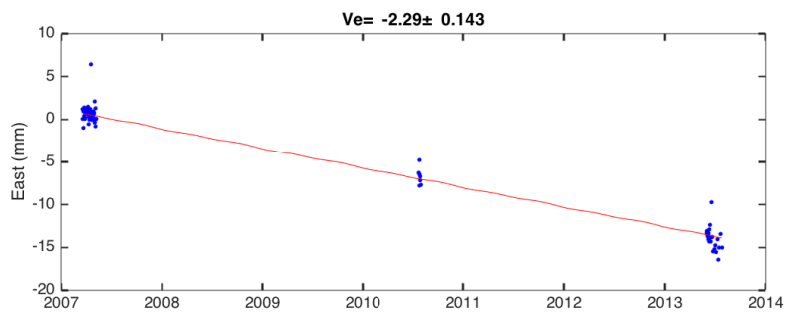
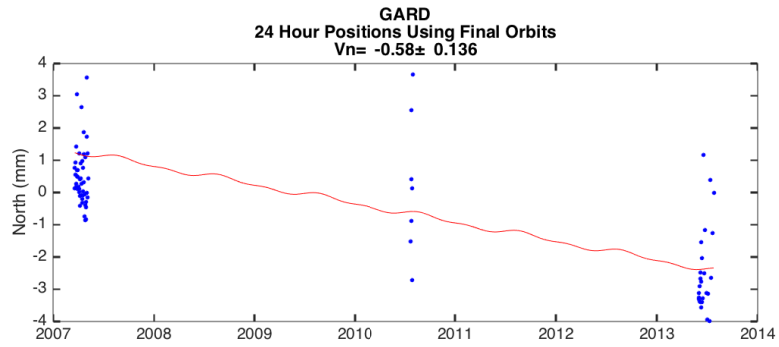
gray dashed line = time of nearby earthquake  
cyan dashed line = time of known equipment change  
last data on 27-May-2014  
Processed and Plotted by the Nevada Geodetic Laboratory on 26-Jun-2014



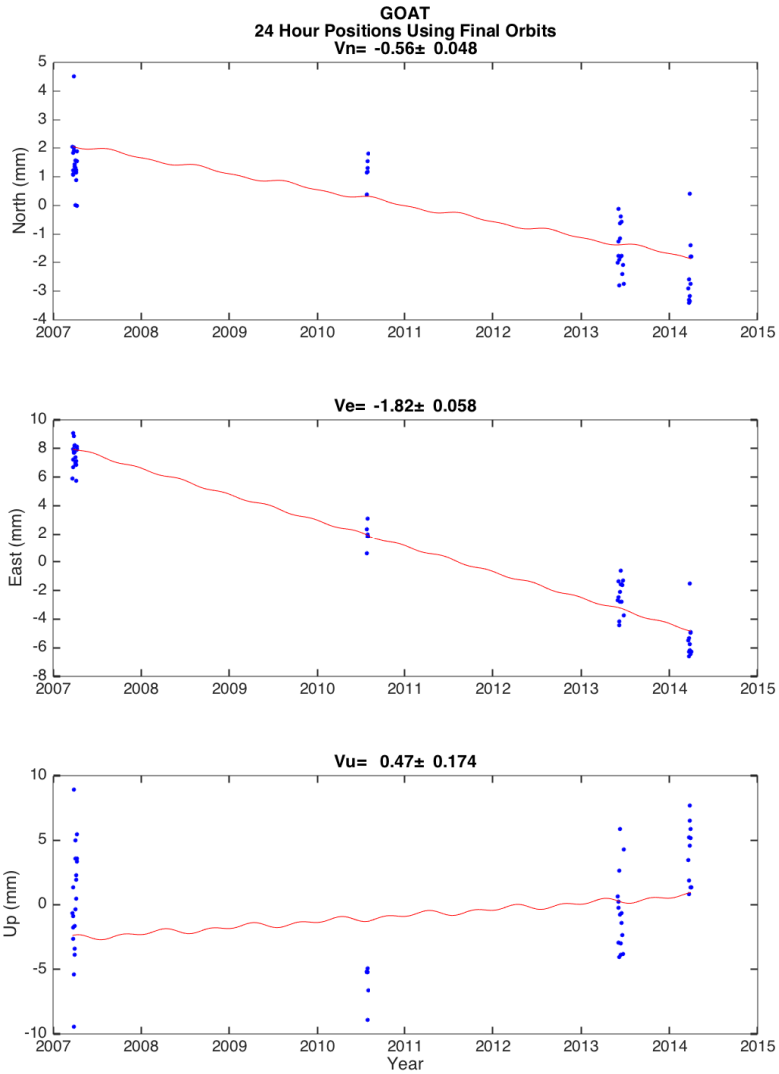
last data on 05-May-2014  
 Processed and Plotted by the Nevada Geodetic Laboratory on 26-Jun-2014



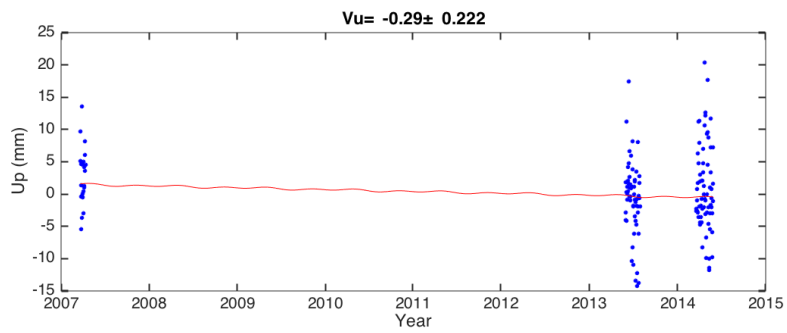
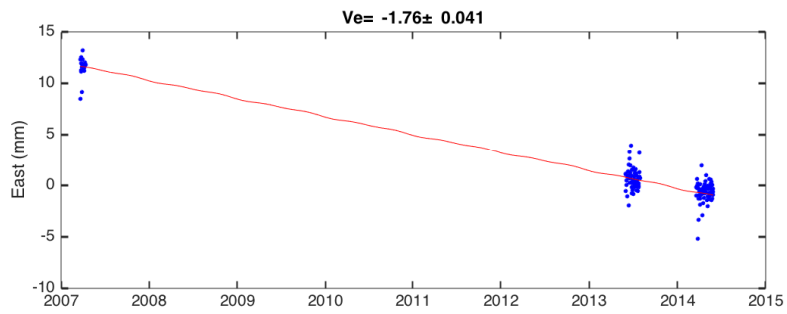
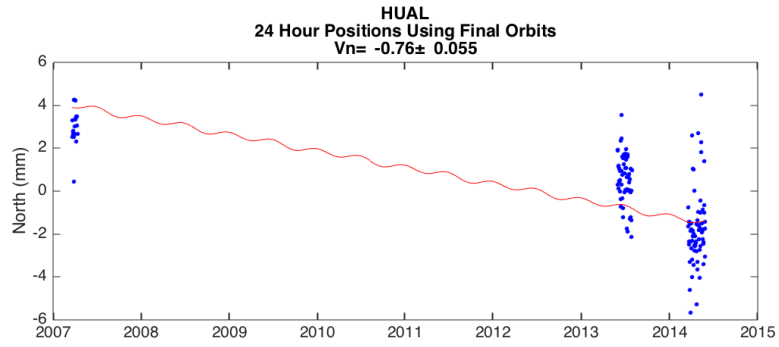
last data on 28-Jul-2013  
 Processed and Plotted by the Nevada Geodetic Laboratory on 26-Jun-2014



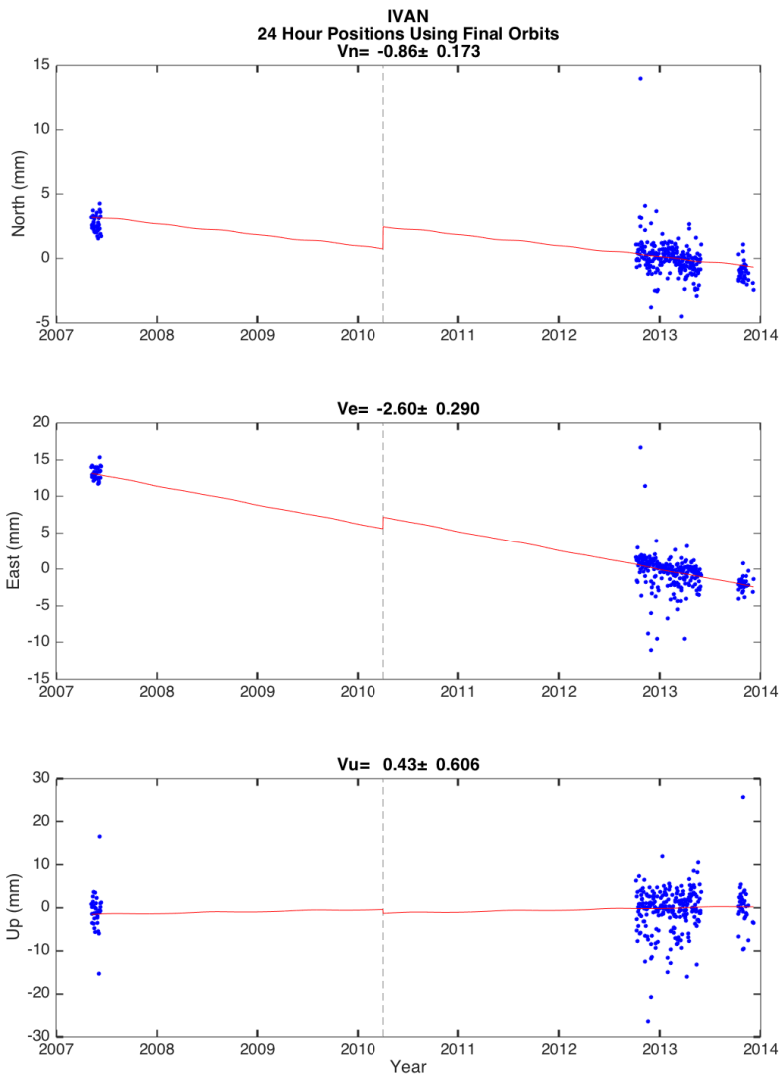
last data on 25-Jul-2013  
 Processed and Plotted by the Nevada Geodetic Laboratory on 26-Jun-2014



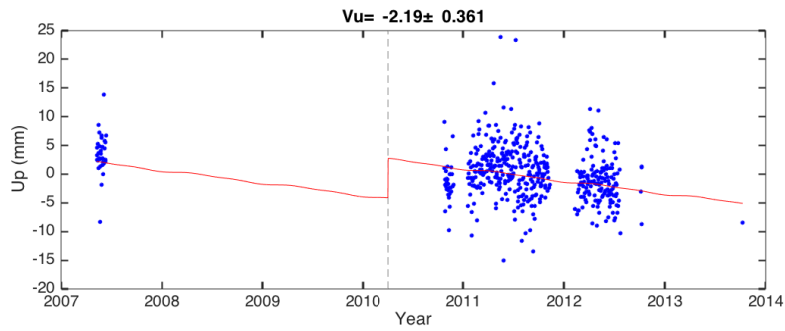
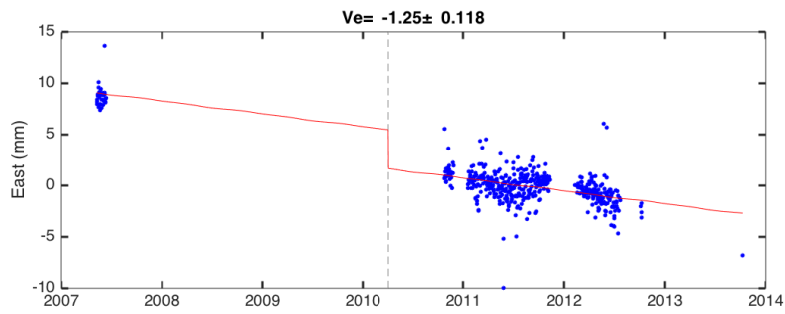
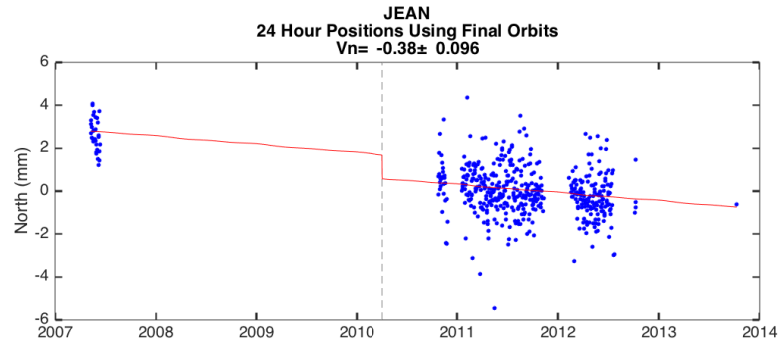
last data on 30-Mar-2014  
 Processed and Plotted by the Nevada Geodetic Laboratory on 26-Jun-2014



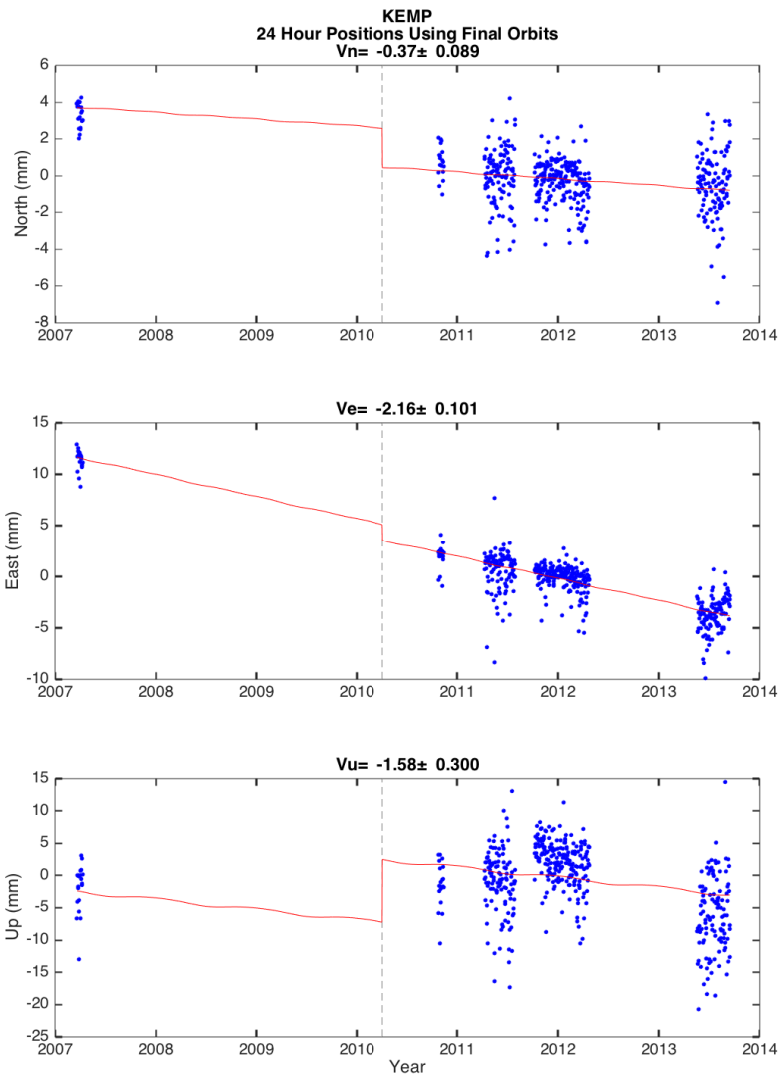
last data on 28-May-2014  
 Processed and Plotted by the Nevada Geodetic Laboratory on 26-Jun-2014



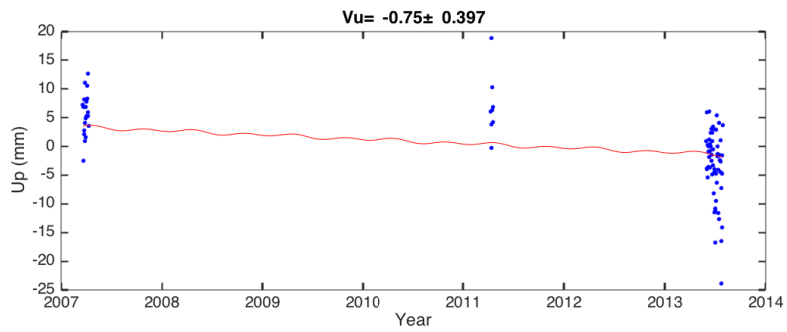
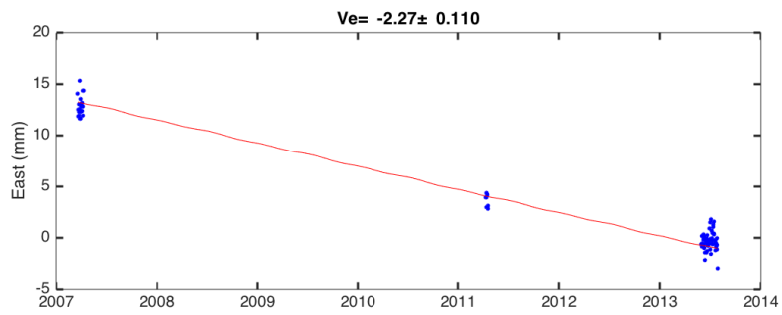
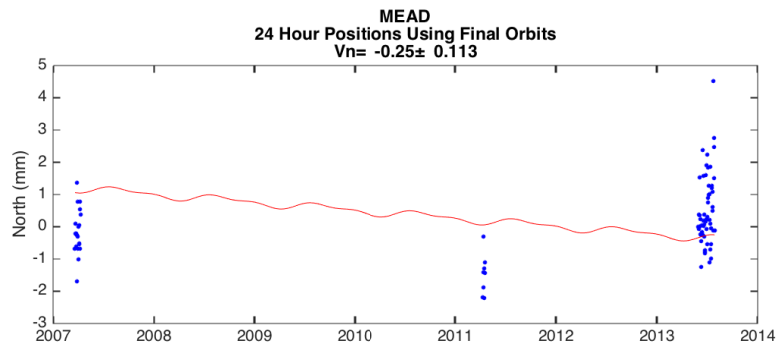
gray dashed line = time of nearby earthquake  
cyan dashed line = time of known equipment change  
last data on 05-Dec-2013  
Processed and Plotted by the Nevada Geodetic Laboratory on 26-Jun-2014



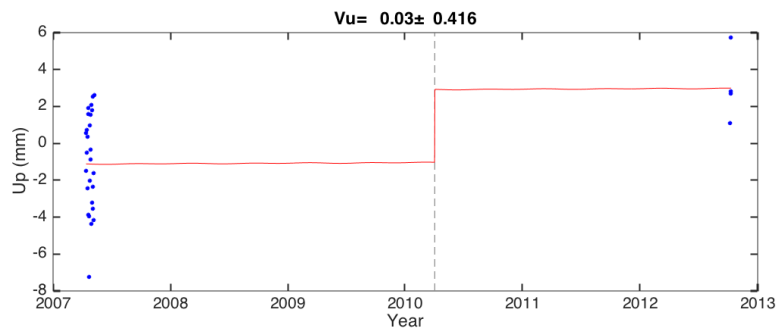
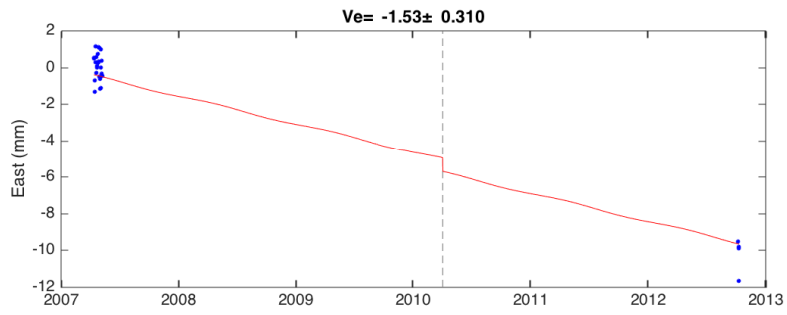
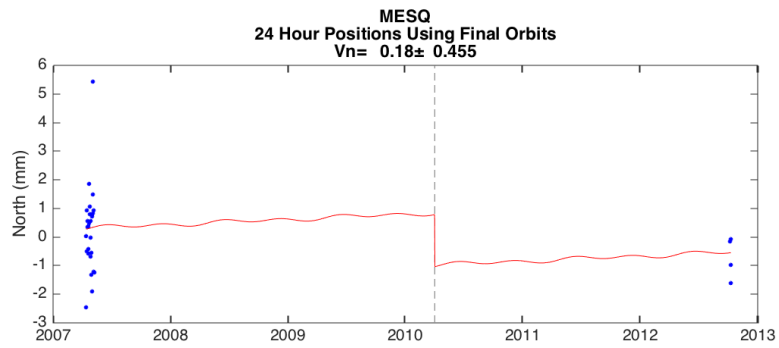
gray dashed line = time of nearby earthquake  
 cyan dashed line = time of known equipment change  
 last data on 09-Oct-2013  
 Processed and Plotted by the Nevada Geodetic Laboratory on 26-Jun-2014



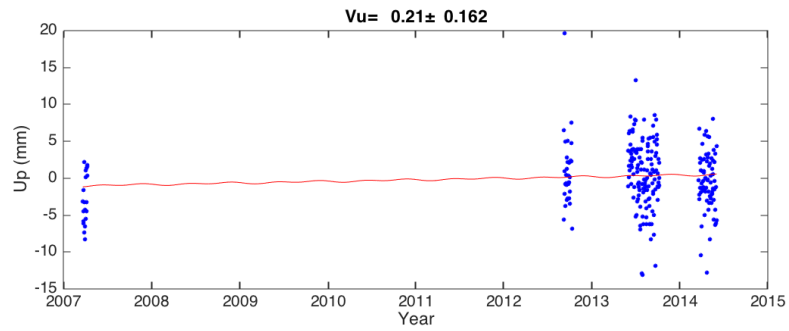
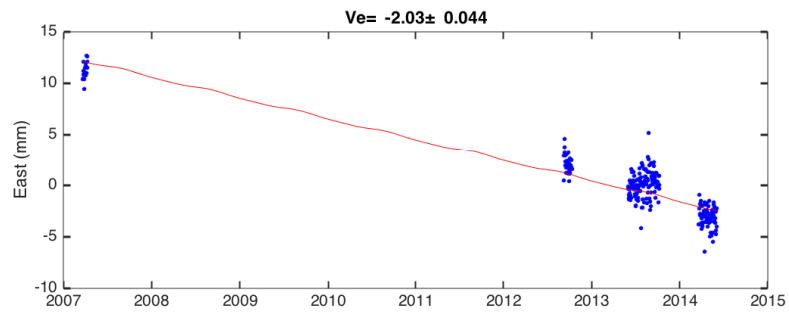
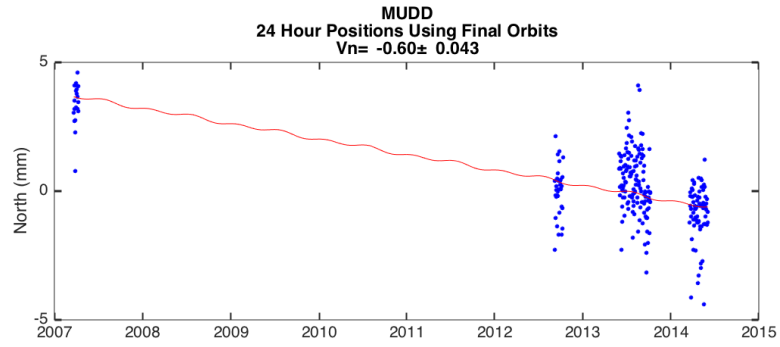
gray dashed line = time of nearby earthquake  
cyan dashed line = time of known equipment change  
last data on 14-Sep-2013  
Processed and Plotted by the Nevada Geodetic Laboratory on 26-Jun-2014



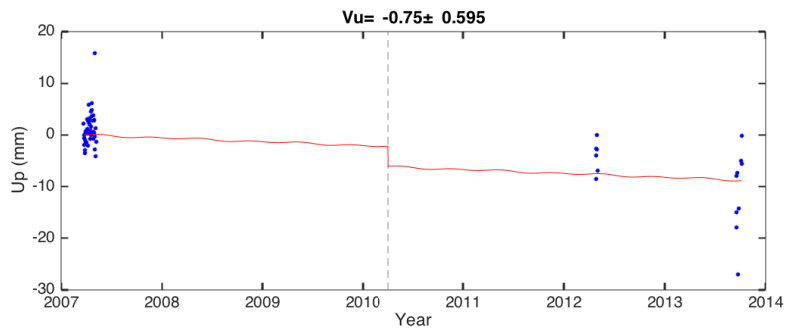
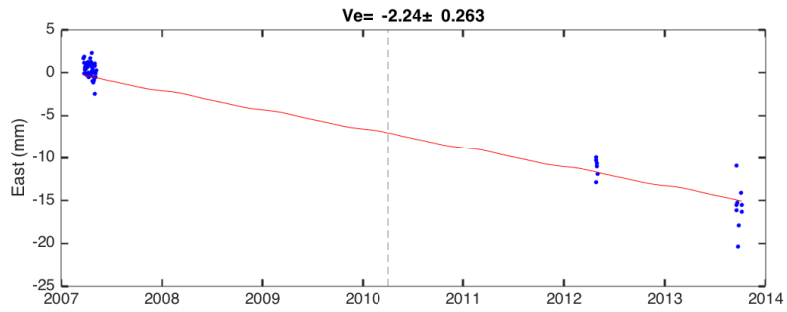
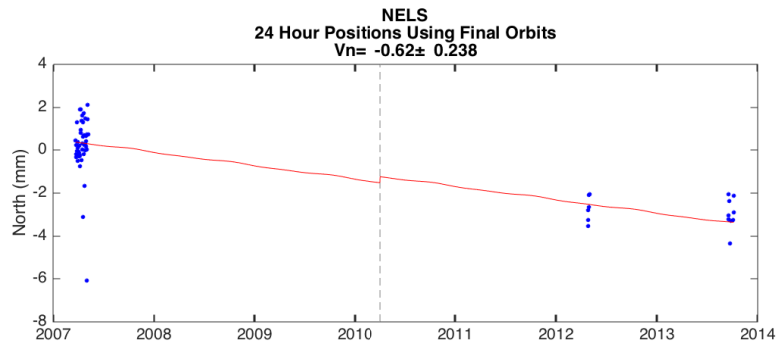
last data on 28-Jul-2013  
 Processed and Plotted by the Nevada Geodetic Laboratory on 26-Jun-2014



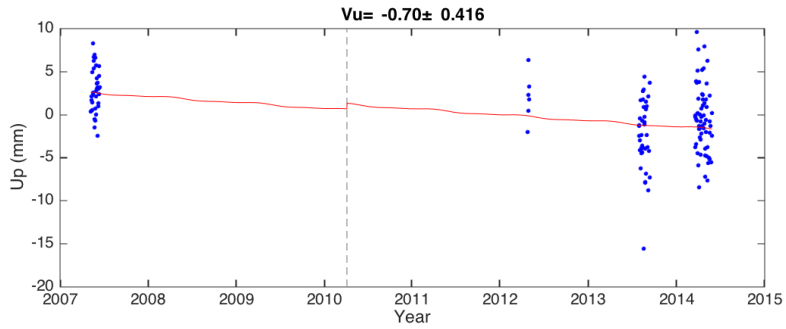
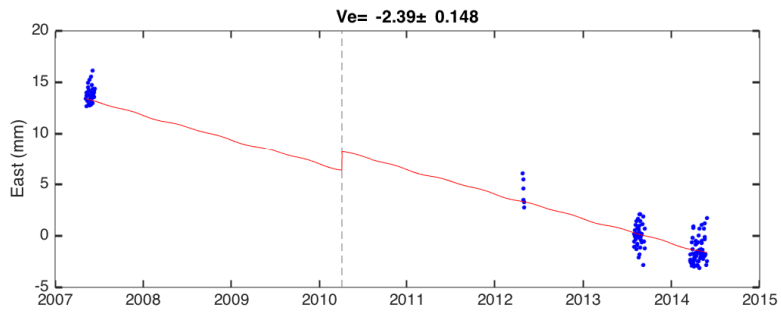
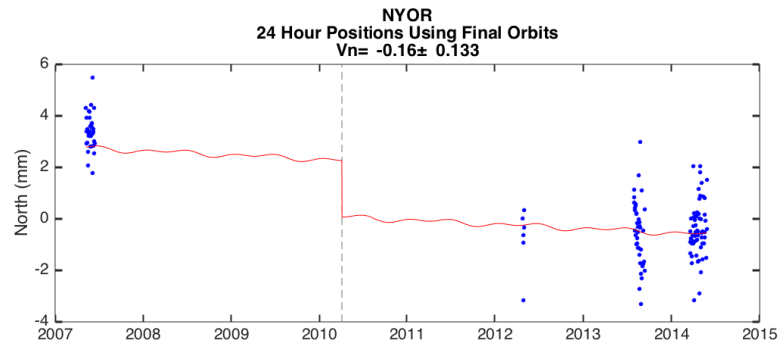
gray dashed line = time of nearby earthquake  
cyan dashed line = time of known equipment change  
last data on 09-Oct-2012  
Processed and Plotted by the Nevada Geodetic Laboratory on 26-Jun-2014



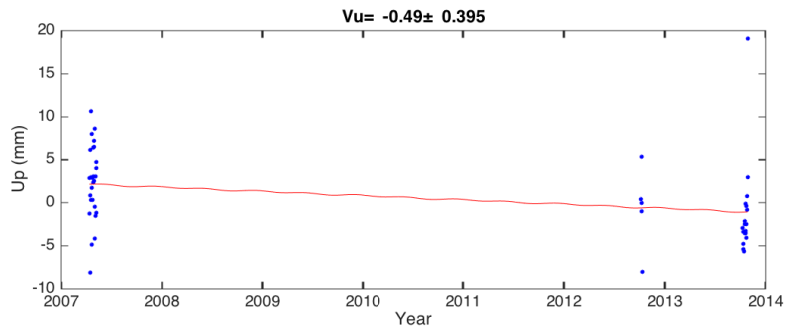
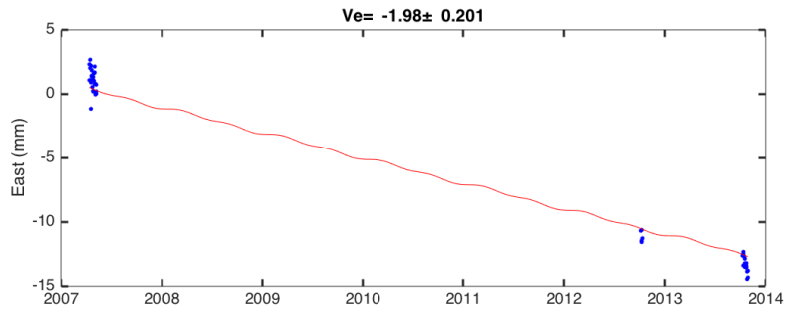
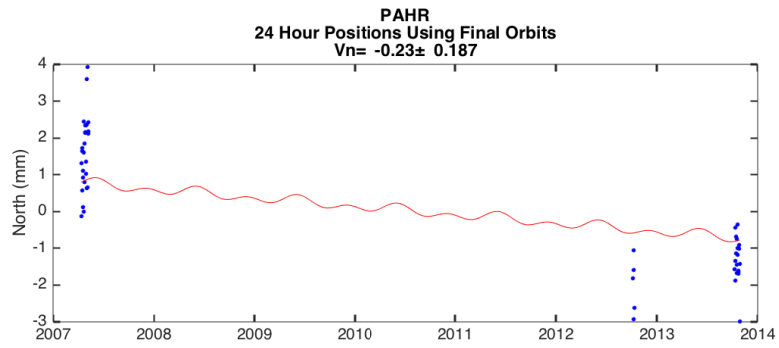
last data on 02-Jun-2014  
Processed and Plotted by the Nevada Geodetic Laboratory on 26-Jun-2014



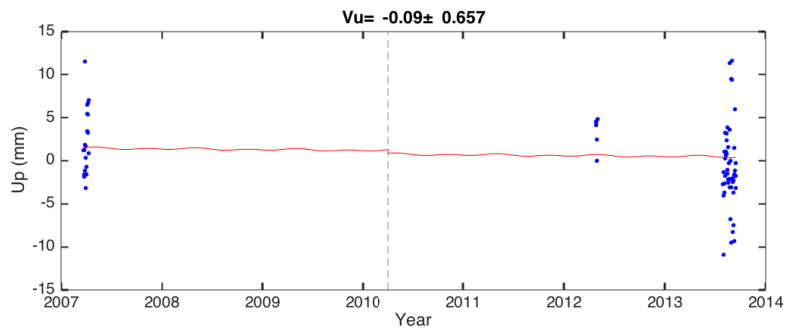
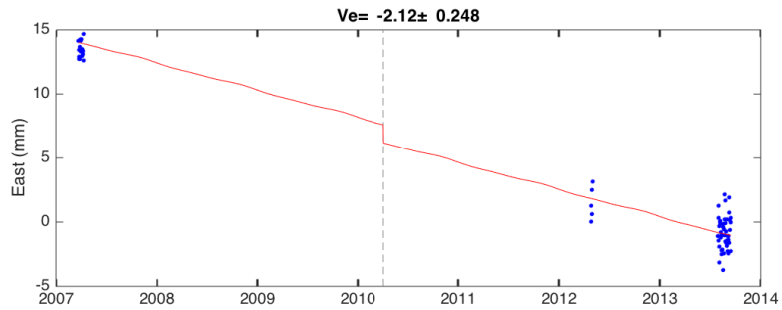
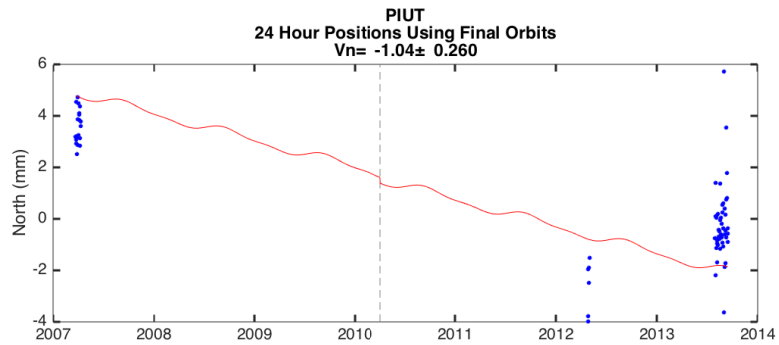
gray dashed line = time of nearby earthquake  
 cyan dashed line = time of known equipment change  
 last data on 05-Oct-2013  
 Processed and Plotted by the Nevada Geodetic Laboratory on 26-Jun-2014



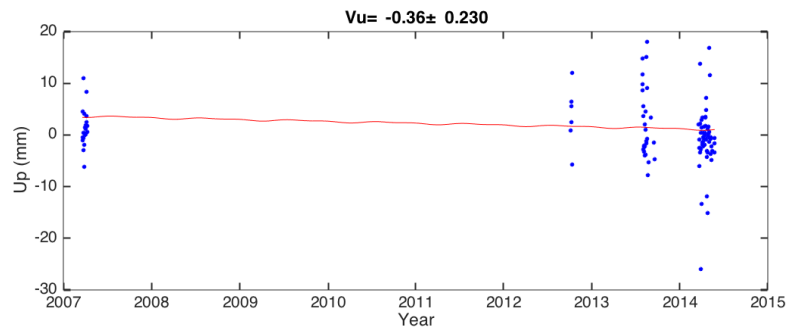
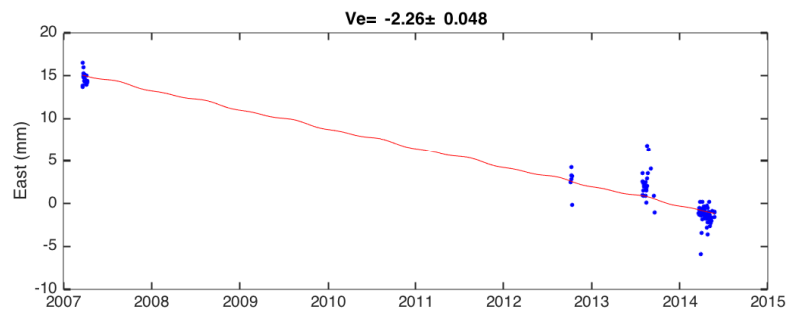
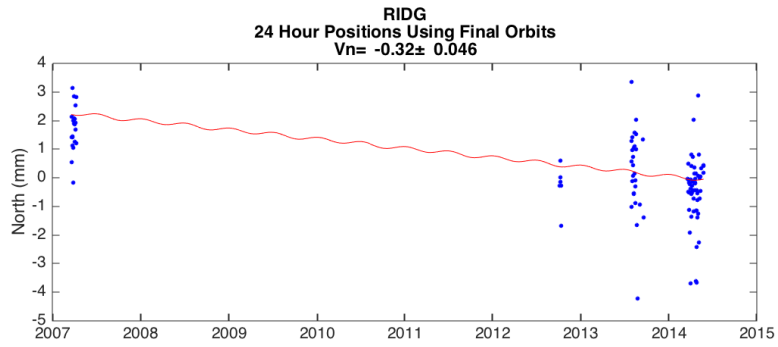
gray dashed line = time of nearby earthquake  
 cyan dashed line = time of known equipment change  
 last data on 27-May-2014  
 Processed and Plotted by the Nevada Geodetic Laboratory on 26-Jun-2014



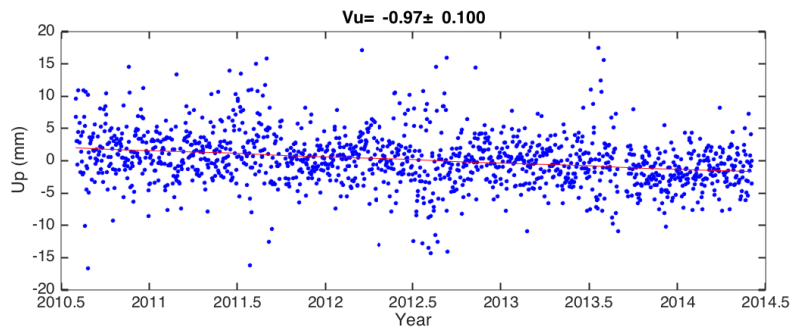
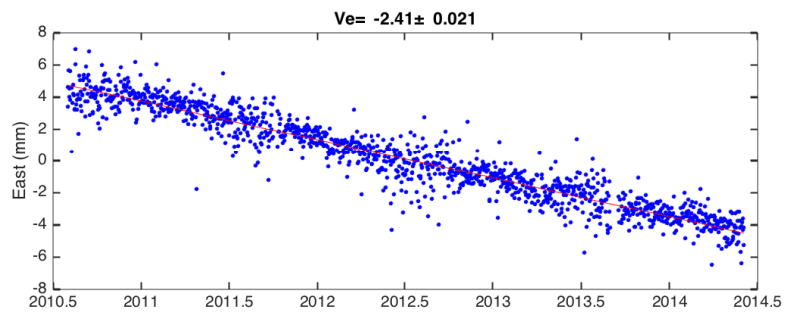
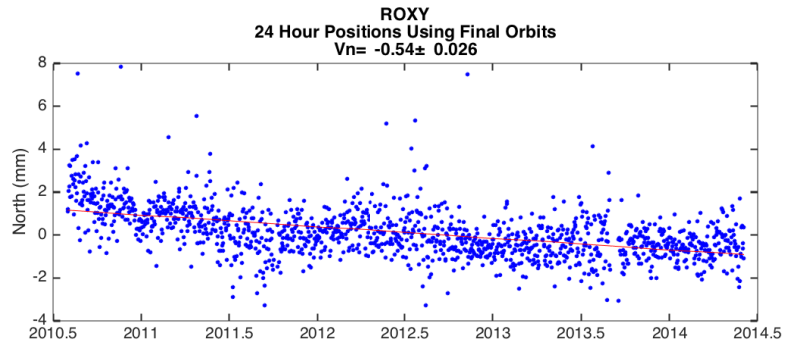
last data on 27-Oct-2013  
 Processed and Plotted by the Nevada Geodetic Laboratory on 26-Jun-2014



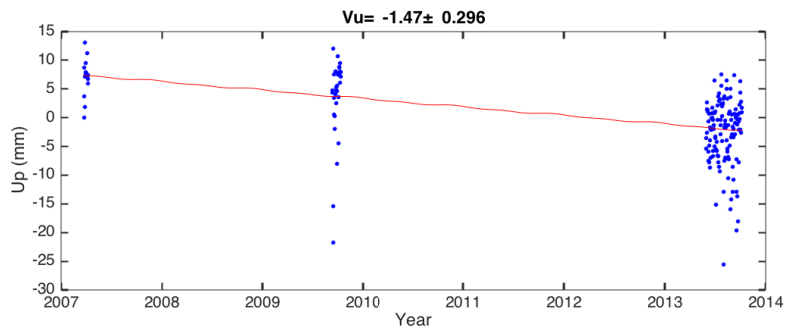
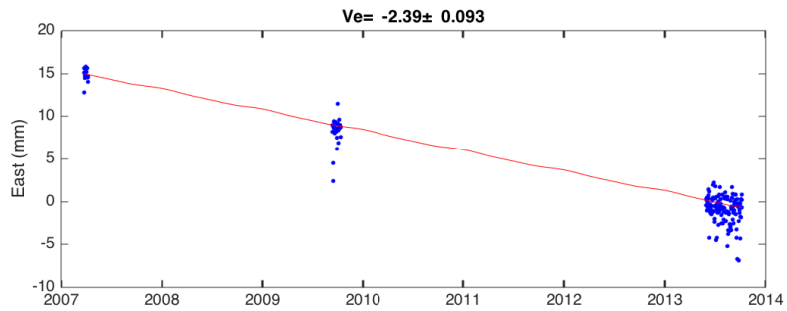
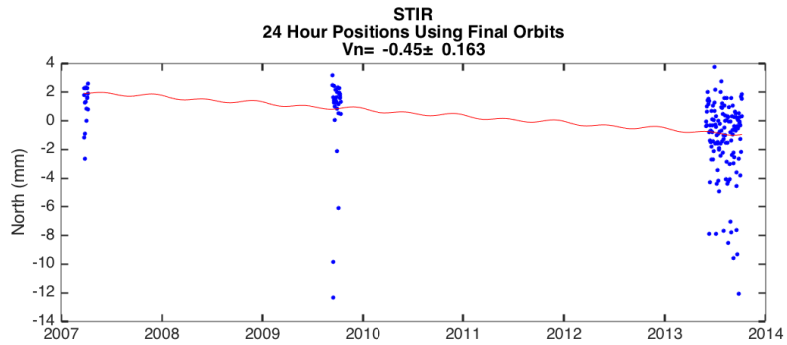
gray dashed line = time of nearby earthquake  
 cyan dashed line = time of known equipment change  
 last data on 14-Sep-2013  
 Processed and Plotted by the Nevada Geodetic Laboratory on 26-Jun-2014



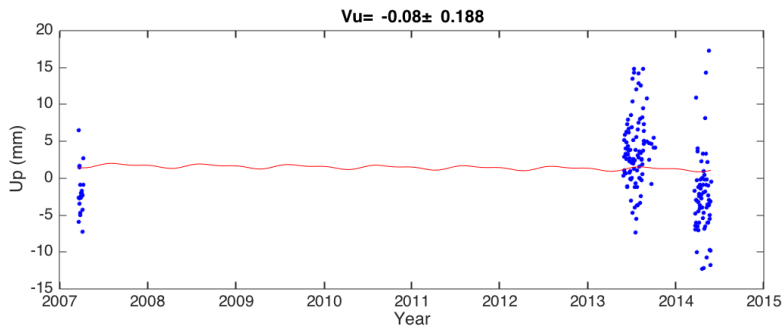
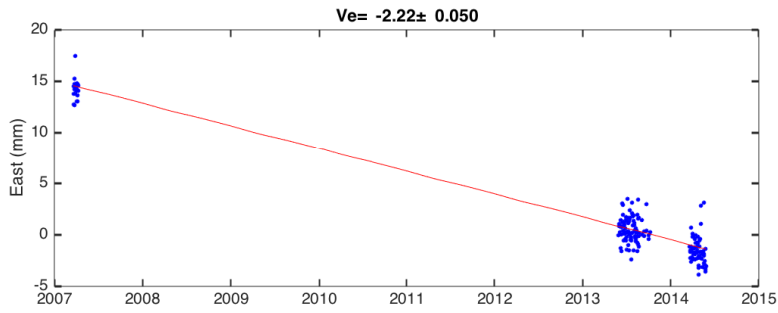
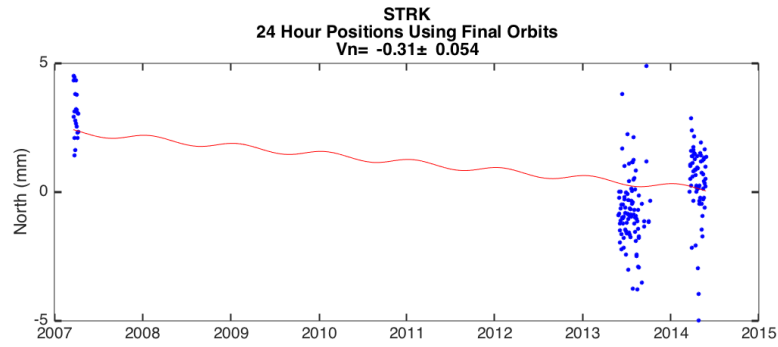
last data on 25-May-2014  
 Processed and Plotted by the Nevada Geodetic Laboratory on 26-Jun-2014



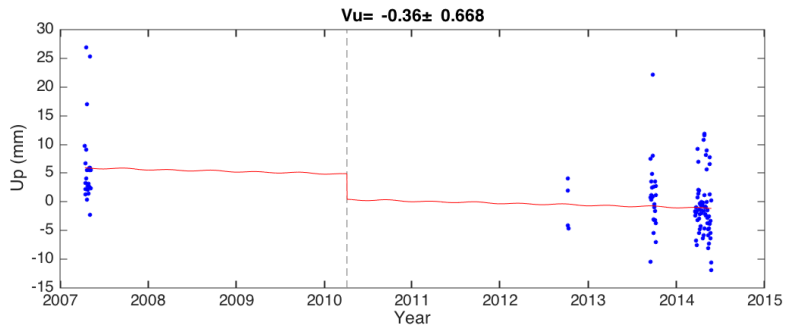
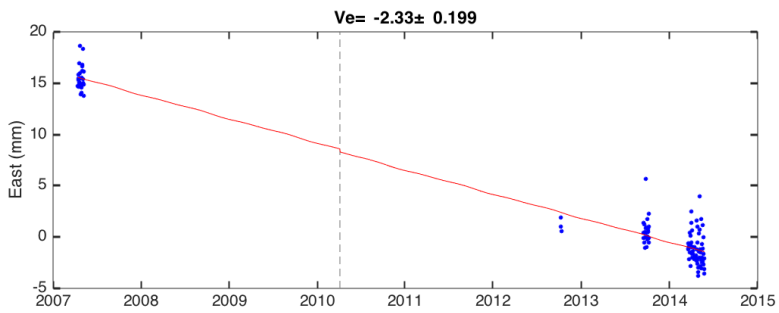
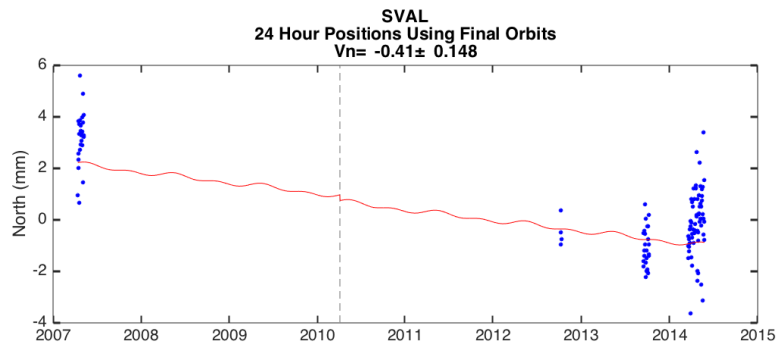
last data on 03-Jun-2014  
Processed and Plotted by the Nevada Geodetic Laboratory on 26-Jun-2014



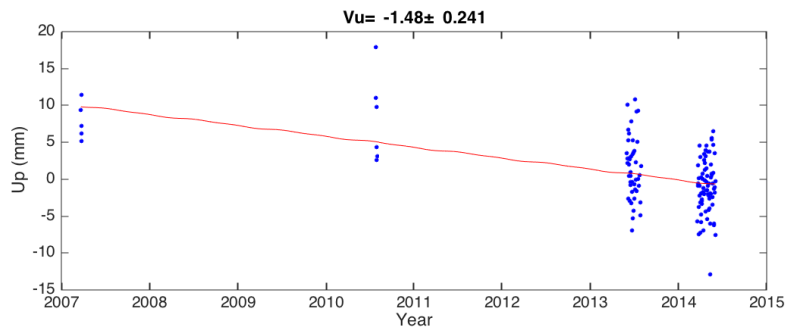
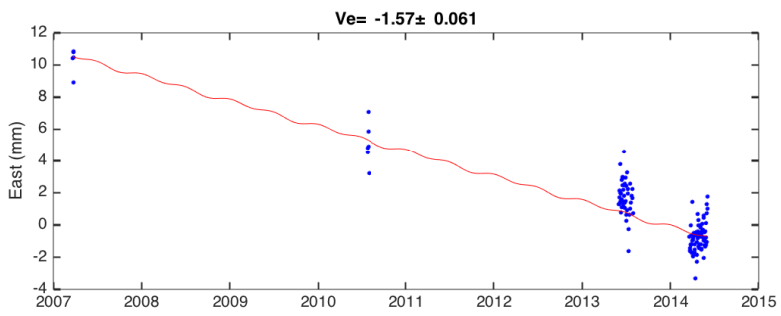
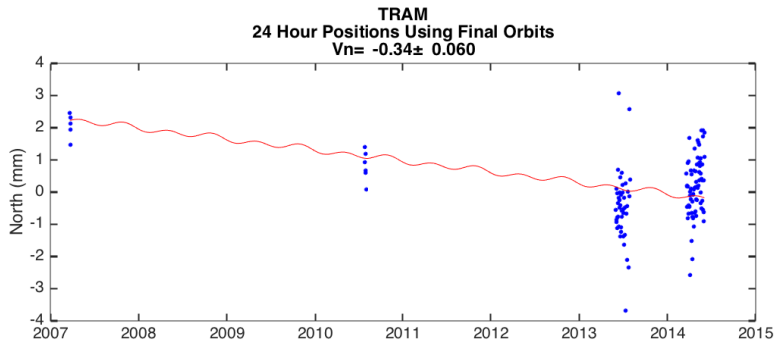
last data on 06-Oct-2013  
 Processed and Plotted by the Nevada Geodetic Laboratory on 26-Jun-2014



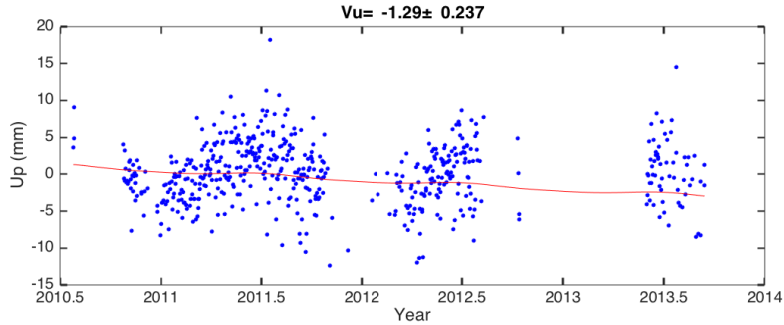
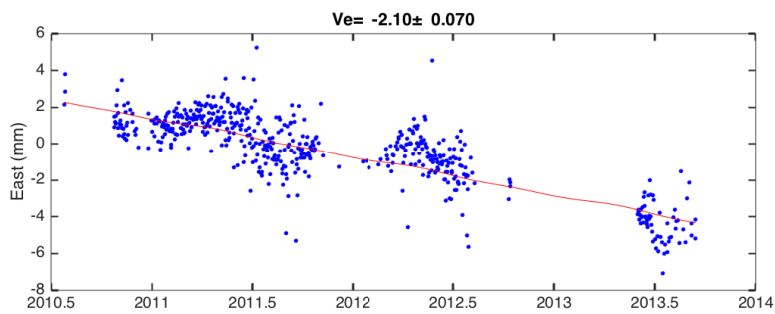
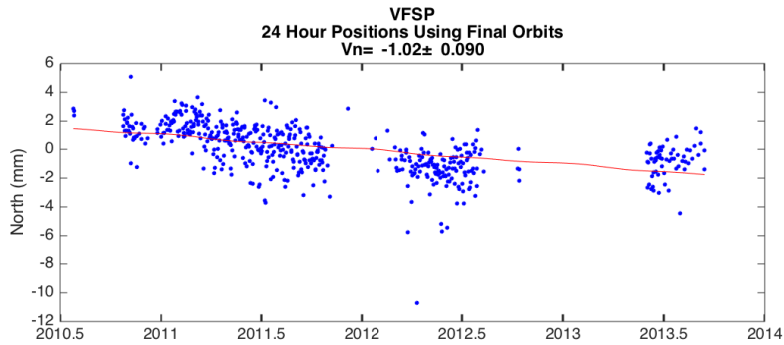
last data on 26-May-2014  
 Processed and Plotted by the Nevada Geodetic Laboratory on 26-Jun-2014



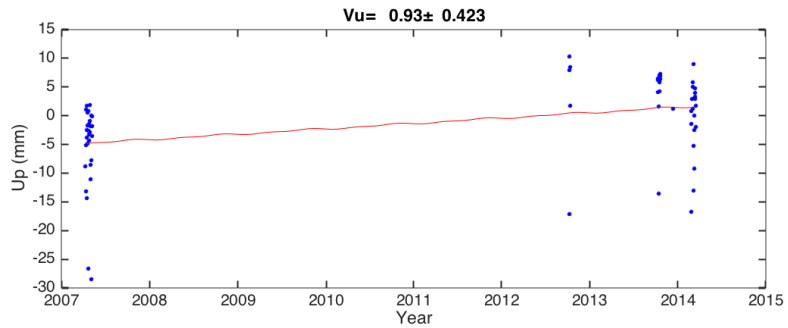
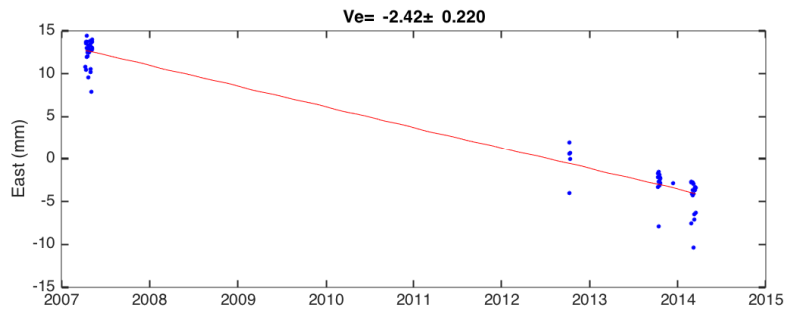
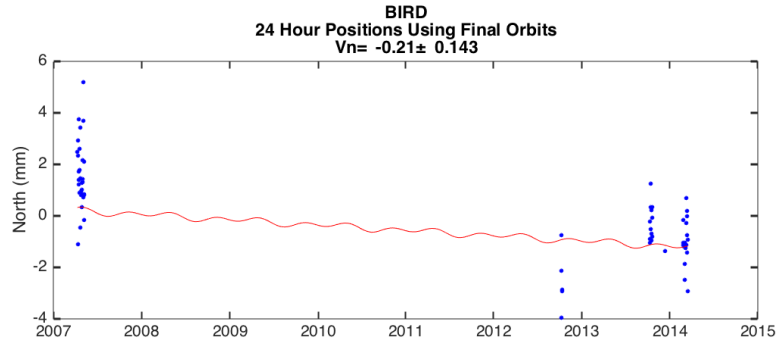
gray dashed line = time of nearby earthquake  
 cyan dashed line = time of known equipment change  
 last data on 25-May-2014  
 Processed and Plotted by the Nevada Geodetic Laboratory on 26-Jun-2014



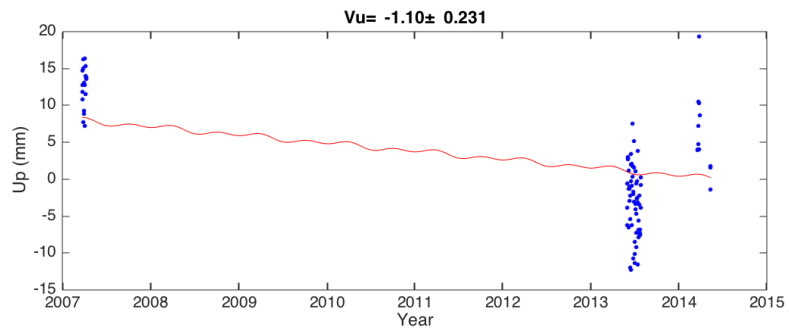
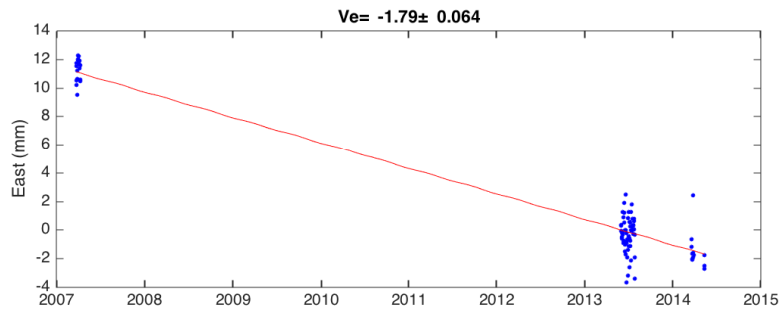
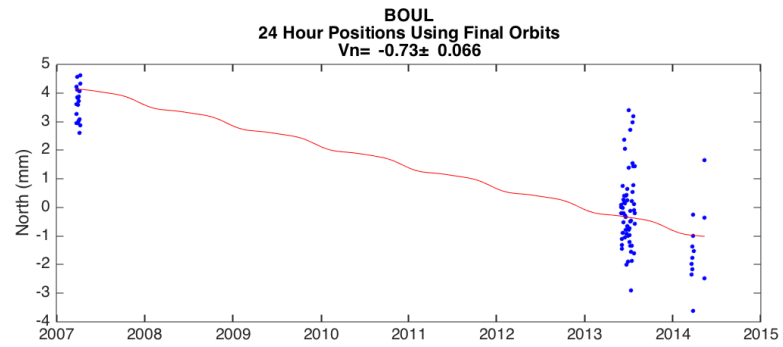
last data on 02-Jun-2014  
 Processed and Plotted by the Nevada Geodetic Laboratory on 26-Jun-2014



last data on 13-Sep-2013  
 Processed and Plotted by the Nevada Geodetic Laboratory on 26-Jun-2014



last data on 16-Mar-2014  
 Processed and Plotted by the Nevada Geodetic Laboratory on 26-Jun-2014



last data on 12-May-2014  
 Processed and Plotted by the Nevada Geodetic Laboratory on 26-Jun-2014